

Organic/Inorganic Hybrid Composites from Cubic Silsesquioxanes. Epoxy Resins of Octa(dimethylsiloxyethylcyclohexylepoxyde) Silsesquioxane

Jiwon Choi,[†] Albert F. Yee,[‡] and Richard M. Laine^{*,§,‡}

Department of Materials Science and Engineering, and The Macromolecular Science and Engineering Center, University of Michigan, Ann Arbor, Michigan 48109-2136, and Institute of Materials Research & Engineering, 3, Research Link, Singapore 117602

Received March 14, 2003

ABSTRACT: Standard research protocols were developed to explore the use of octahedral silsesquioxane (cube) organic/inorganic nanocomposites as model systems for determining nanostructure–processing–property relationships to demonstrate that nanoscale structural manipulation of the organic component can significantly change macroscale physical properties. Comparison of octaglycidyl dimethylsiloxy octasilsesquioxane [(glycidyl-Me₂SiOSiO_{1.5})₈] (OG)/diaminodiphenylmethane (DDM) and octa(ethylcyclohexylepoxyde)dimethylsiloxy silsesquioxane (OC)/DDM nanocomposite resins provide the first demonstration that well-defined nanostructures can be formed wherein linear organic tethers of known structure join only two cube vertices. HF dissolution of cubes followed by GPC analysis demonstrates that only linear tethers form in OC/DDM. TEM studies suggest that these nanocomposites are homogeneous at the nanometer scale, thus supporting the chemical analysis studies. The physical properties of these nanocomposites were then systematically assessed and the network tether architectures quantitatively analyzed to correlate the changes in nanostructure with macroscopic properties. TGA, DMA, room-temperature mechanical properties, and molecular modeling studies suggest that nanocomposite thermomechanical properties can be modified by changing the tether architecture/rigidity and predicted by molecular modeling. Surprisingly, OC/DDM elastic moduli increase from 2.2 to 3.3 GPa as the DDM content increases 2-fold beyond the maximum cross-link density into a high defect density region while the fracture toughness remains unchanged. An explanation for this behavior is proposed. This appears to be a true nanocomposite property. Blending provides an effective approach for modifying properties dominated by particular tethers. The results reported here offer several guidelines in designing cube hybrid nanocomposites and detailing future studies.

Introduction

Organic/inorganic hybrid nanocomposites are currently under intense study as next generation materials because they offer the potential to realize novel properties and to design/tailor these properties extensively.^{1–10} Nanocomposite properties arise primarily from a synergistic combination of individual organic/inorganic component properties when these components are mixed intimately. This is particularly true when the component sizes approach the nanometer scale. Here, nanocomposite properties often do not comply with estimates from the rule of mixture because of extensive interfacial interactions. As properties of interest extend from thermomechanical^{9–13} to barrier,^{14–16} electronic,^{17–19} and photonic^{20–23} properties, more diverse organic/inorganic elements^{5,24–27} are being examined.

Of equal importance in developing advanced materials is the capability of predicting/tailoring/controlling properties. The best strategy for this purpose is to construct nanocomposites by assembling the smallest components exhibiting distinct properties. Motivation for this approach is that control of molecular structure and properties at the smallest scale offers optimal control of macroscale properties. However, this approach requires an excellent understanding of the relationships between the components, their organization during and

after processing, and resulting macroscopic properties in order to select the best components and processing conditions to realize target properties. Although significant advances have been made in nanocomposite development, understanding structure–processing–property relationships remains a serious scientific challenge.

The systematic study of such relationships can start by “building” and understanding well-defined model systems wherein nanocomponents with distinct properties are selectively and systematically varied and macroscopic properties characterized in relation to changes in these variations. In this light, we have begun to explore octafunctionalized cubic silsesquioxanes (cubes) as building blocks for nanocomposites.^{28–36}

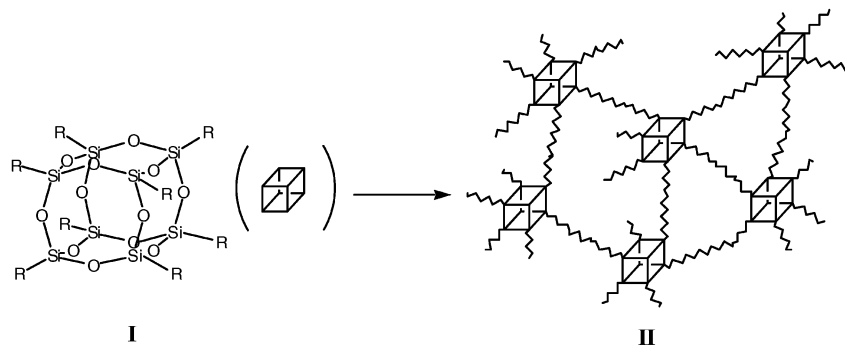
In cubic macromonomers, all eight vertices are functionalized and equally reactive. Upon processing, the size of the cube core (0.53 nm) and the functionalized arms (1–2 nm depending on the structure) define the size of the organic/inorganic components in the resulting nanocomposites where both components are distributed uniformly and periodically. Various polymer segments can be incorporated in organic tethers, and their nanoarchitectures modified easily to change macroscopic behavior while the cube cores behave as nanosized, rigid inorganic cross-linkers dispersed uniformly throughout the composite. The cube cores represent the “constant” in the equation that defines macroscopic properties. Then, tether manipulation enables one to selectively vary nanocomposite construction variables at the smallest scale offering numerous sets of nanosystems for comparative study.

[†] The Macromolecular Science and Engineering Center, University of Michigan.

[‡] Institute of Materials Research & Engineering.

[§] Department of Materials Science and Engineering, University of Michigan.

Scheme 1. Formation of Nanocomposites with a Uniform Distribution of Cubic Silsesquioxane (I) Units in a Periodic Matrix (II) via Crosslinking of Functional Groups (R)



Silsesquioxane nanocomposites also offer potential for novel properties because uniformly dispersed organic/inorganic components at the nanoscale can synergistically change bulk properties. Scheme 1 illustrates the formation of nanocomposites from functionalized cubic silsesquioxanes. Our initial synthetic objectives targeted routes to structures **II** that produce completely discontinuous nanocomposites^{28–29,37–38} That is, the reaction chemistry used to produce the nanocomposite must generate organic tethers that join cube vertices but do not copolymerize.

With synthetic protocols for providing nanobuilding blocks with tailored organic tethers in place,^{30,32–36} we initiated studies to develop synthesis-processing-properties relationships to establish complete nanocomposite construction guidelines. Our practical goals are to (1) establish a comprehensive picture of nanocomposite behavior; (2) identify design, synthesis, and processing parameters to optimize properties; and (3) develop procedures to predict/tailor/control properties.

The initial objectives were to prove that cube nanocomposites indeed consist of well-defined nanosized building components periodically arranged within the composite and to develop standard test and analytical procedures to characterize these nanostructures and properties. Because there are many construction parameters to vary, our practical goal was to develop and analyze simple systems where only one or two parameters are varied selectively in a constant environment and the changes in nanostructure and properties monitored.

To this end, we identified epoxy resin cure chemistry as a method of making completely discontinuous nanocomposites. Thus, cubes terminated with epoxy groups could be linked using an aromatic amine as a curing agent to form tethers.^{28,29} Once the functional group and cure chemistry were fixed, small changes in “construction” parameters including tether length, rigidity and the chemical structure and their effects on physicochemical properties were assessed to establish selected structure–processing–property relationships.

Our previous work on the octaglycidyl dimethylsiloxy-octasilsesquioxane [(glycidyl)-Me₂SiO_{1.5}]₈ (OG)/diaminodiphenylmethane (DDM) system²⁹ established the above-described baseline processing methods and characterization procedures to create standard protocols for studying this family of nanocomposites. In this work, we demonstrated that (1) epoxy resin nanocomposites are truly well-defined in terms of chemical bonding/structural periodicity and are completely discontinuous at the nanoscale, (2) the tether structure can be con-

trolled by varying the stoichiometry and the cross-linking chemistry, and (3) cross-link density and tether structure strongly affect thermomechanical properties.

Here, we present a second study that demonstrates that selective modification of tether structure and rigidity in cube nanocomposites can produce significantly different thermomechanical properties. This is the first proof, in our studies, that appears to demonstrate that nanoarchitecture manipulation can strongly affect the macroscopic behavior of nanocomposites. In practice, the octa(ethylcyclohexylepoxidedimethylsiloxy) silsesquioxane (OC)/DDM nanocomposites studied here differ from OG/DDM only by one CH₂ that forms a ring in each tether; although the number of atoms between the core and the epoxy ring remain the same.

In this study, we compare the curing and thermo-mechanical behavior of OC/DDM with that of OG/DDM using the same cross-linking agent (DDM) and the same processing conditions. Thus, any potential differences in behavior should be attributable to these tether structure changes. The comparative study presented here permits useful conclusions to be drawn about nanostructure–macroscopic property relationships. A preliminary report was published.²⁸

Experimental Section

Materials. Tetramethylammonium hydroxide (25 wt % in MeOH), tetraethoxysilane, dimethylchlorosilane, 4-vinyl-1,2-cyclohexene epoxide, dicyclopentadiene, hydrated chloroplatinic acid, glacial acetic acid, and triphenylphosphine were purchased from Aldrich (Milwaukee, WI) and used without further purification. 4,4'-Diaminodiphenylmethane (DDM) was purchased from Alfa Aesar (Ward Hill, MA) and used as received.

Syntheses. Catalyst. Platinum dicyclopentadiene [Pt(dcp)] was synthesized following a literature procedure.³⁹ Hydrated chloroplatinic acid 500 mg (3.78 mmol) was dissolved in 1.1 mL of glacial acetic acid in a 25 mL reaction flask, and the solution was further diluted with 2 mL of water under N₂. The mixture was then heated to 70 °C and 0.4 mL of dicyclopentadiene added. The solution was stirred vigorously for 24 h at 70 °C and then cooled. The solid product was filtered off, decolorized with charcoal, and recrystallized from THF to give 190 mg (yield 51%).

Octa(ethylcyclohexylepoxidedimethylsiloxy)silsesquioxane (OC). OC was synthesized in three steps. First, octaanion solution [(⁻OSiO_{1.5})₈] was prepared by mixing 804 mL of Me₄NOH (25 wt % in methanol) (7.64 mol), 391 mL of methanol and 293 mL of deionized water followed by dropwise addition of 428 mL of Si(OEt)₄ (1.18 mol) under N₂. Octahydrido “spacer” cube [H(CH₂)₂SiOSiO_{1.5}]₈ was then made by reaction of 600 mL of octaanion with 262 mL (2.6 mol) of

Table 1. GPC Data of OC and OG

	calcd ^a	M_n	M_w	PDI ^b
OC	2011	1341	1370	1.02
OG ²⁹	1931	1514	1546	1.02

^a Theoretical molecular weight. ^b Polydispersity index.

Table 2. Compositions of OC/DDM Composites

	OC						
	0.5	0.75	1	1.25	1.5	1.75	2
N							
wt % DDM	16.4	22.8	28.3	33.0	37.2	40.8	44.1
Phr ^a DDM	19.6	29.6	39.4	49.3	59.2	69.0	78.8

^a Phr: Parts of DDM per hundred of OC resin by weight.^{40–44}

dimethylchlorosilane in 1500 mL of hexane for 2 h. Finally, OC was prepared via hydrosilylation^{28,29} of 4-vinyl-1,2-cyclohexene-epoxide, with octahydrido spacer cube using Pt(dcp) as catalyst.

Product purity was confirmed by ¹H NMR. Molecular masses and distributions were measured by GPC as in Table 1. In this table, OG²⁹ data are also shown for comparison. Because the hydrodynamic volumes of "spherical" OC and OG are smaller than the linear polystyrenes used for GPC calibration, their measured molecular weights were smaller than the theoretical values. Also, OG appears even larger than OC, despite the smaller theoretical molecular weight, because flexible OG tethers occupy larger volumes than OC in GPC measurements at room temperature.

Curing Optimization Tests. In our previous studies, we found that curing for 6 h at 150 °C was sufficient to obtain consistent room-temperature moduli for OG/DDM. However, curing at 150 °C for at least 10 h was necessary for OC/DDM. Therefore, it was decided that identical cure conditions of 150 °C/10 h/N₂ would be adopted for OC/DDM and OG/DDM for comprehensive comparative studies.

Nanocomposites Preparation. In formulating OC/DDM composites, a variable *N* was defined as

$$N = \frac{\text{number of amine groups in DDM}}{\text{number of epoxy rings in OC}}$$

Thus, when *N* = 1, there are equal numbers of NH₂ groups and epoxy rings in the resin. Conventional epoxy resin formulations use *N* = 0.5 ratios.^{40–44} Table 2 shows OC/DDM formulations with various *N*s. Epoxy formulation conventions measure curing agents according to Phr (parts of amines per hundred of resins; ratio of amine weights vs epoxy weights), and thus these values are included for comparison. The total mass of the mixture for each sample was kept constant at 12 g.

Materials were weighed into an aluminum pan (61.5 mm diameter × 18 mm) and mixed by hand. The mixture was melted and degassed at 140–150 °C under vacuum for 7–15 min. When the mixture became homogeneous and no more bubbles emerged, it was poured into an aluminum mold previously surface-coated with Teflon mold release agent and preheated to 150 °C. The mixture was then cured at 150 °C/10 h/N₂. After the mold cooled, the sample was removed and kept in a desiccator prior to testing.

Preparation of Nanocomposites with Improved Mechanical Properties. Nanocomposites with improved mechanical properties were prepared by mixing OG and OC at *N* = 1.25. OG and OC were weighed into the same aluminum pan (61.5 mm diameter × 18 mm), preheated at 140–150 °C for 2–3 min to melt OC and form a liquid solution by hand mixing. DDM was then added and melted followed by additional mixing by hand. The final mixture was degassed at the same temperature under vacuum for 7–15 min and cured following the same methods as above. The total mass of the mixture was kept constant at 12 g. Table 3 shows the actual formulation of these composites.

Table 3. Blending of OG/OC at *N* = 1.25

	mol % OG in OG/OC mixture					
	0%	25%	50%	65%	75%	100%
OG (g)	0	1.94	3.90	5.11	5.91	7.96
OC (g)	8.05	6.06	4.08	2.87	2.05	0
DDM (g)	3.95	4.00	4.02	4.02	4.04	4.04

Characterization. Gel Permeation Chromatography (GPC). Molecular masses and distributions for octahydrido spacer cube and OC were measured using a Waters GPC system, equipped with RI and UV detectors, a Styragel column set (7.8 × 300, HR-high-resolution 0.5, 1, 3, 4), and a PL-DCU data capture unit. These four columns are special units suitable for measuring small molecules including epoxies and amines. The system was calibrated using polystyrene standards. THF was used as the eluent, at a flow rate of 1.0 mL/min. GPC was also used to analyze tether structures following core dissolution (see below).

NMR Analyses. All ¹H NMR analyses were performed with a Varian INOVA 400 spectrometer at 400 MHz with a 6000 Hz spectral width, a relaxation delay of 3.5 s, a pulse width of 38°, and 30K data points. All the spectra were recorded in CDCl₃ using the CHCl₃ signal (7.259 ppm) as an internal reference.

Diffuse reflectance Fourier transform IR spectra (DRIFTS) were obtained using a Mattson Galaxy Series FTIR 3000 spectrometer (Mattson Instruments, Inc.). Optical grade potassium bromide (KBr, International Crystal Laboratories, Garfield, NJ) was used as a background material. Cured sample (5 mg) and KBr crystal (500 mg) were ground together using an alumina mortar and pestle. The ground powder was packed into a sample holder and leveled off with a glass plate to give a smooth surface. The holder was placed in the sample chamber and the spectrum was recorded under dry N₂ purge. At least 128 scans were averaged for each spectrum. The resolution was ±4 cm⁻¹.

Thermal Gravimetric Analysis (TGA). Thermal stabilities of materials were tested under nitrogen or air using a 2960 simultaneous DTA–TGA instrument (TA Instruments, Inc., New Castle, DE). Samples (15–25 mg) were loaded in platinum pans and ramped to 1000 °C (5 °C/min/N₂). The N₂ or air flow rate was 60 mL/min.

Differential Scanning Calorimetry (DSC). Calorimetry was performed on materials using a DSC 2910 (TA Instruments, Inc., New Castle, DE). The N₂ flow rate was 60 mL/min. Sample (10–15 mg) was placed in a pan and ramped to 600 °C (5 °C/min/N₂) without capping. The heat flow differences between the reference blank and the sample pan were recorded.

Tensile Moduli and Fracture Toughness. Fresh samples removed from the aluminum mold had rough edges due to overflow. These edges were polished using a polish wheel with 180, 600, and 1200-grit SiC paper. After polishing, average dimensions were 3.0 × 13.0 × 170.0 mm (errors <±0.2 for width and thickness and <±0.5 for length).

A screw-driven Instron 4502 was used to measure elastic moduli (*E*) and the critical stress intensity factors (*K_{IC}*). Sample dimensions were average values of three points for each sample. The elastic moduli were obtained following ASTM standard E111 (1997), except that the sample geometry was a rectangular bar instead of a dog bone. The ratio of the longitudinal length to the width under tension after clamping was always ≥8 to ensure that ratio of the portion under uniaxial tension was >4. The cross-head speed was set at 1 mm/min. Data were recorded at a speed of 5 points/s. Tests were stopped at loads of 200–250 N. Moduli were measured in the initial elastic deformation region.

The critical stress intensity factor (*K_{IC}*) was measured following ASTM standard E399 (1990) in tension. A 1 mm notch was made on the sample using a hacksaw and a natural crack was introduced using a new razor blade. The ratio of the crack to the width was 0.35–0.55. The sample was then loaded in the Instron and tested until it broke. The load at

fracture was recorded. The critical stress intensity factor was determined from the following equations:

$$K_{IC} = Y\sigma_o a^{1/2}$$

$$Y = \left[1.99 - 0.41\left(\frac{a}{w}\right) + 18.70\left(\frac{a}{w}\right)^2 - 38.48\left(\frac{a}{w}\right)^3 + 53.85\left(\frac{a}{w}\right)^4 \right]$$

$$\sigma_o = \frac{P_b}{Bw}$$

where P_b is the load at the fracture, B is the sample thickness, w is the sample width and a is the crack length.

Dynamic Mechanical Analysis (DMA). The dynamic mechanical behavior of cured samples was studied using a TA instruments 2980 dynamic mechanical analyzer (New Castle, DE). Cured samples were polished to $\approx 3.0 \times 13.0 \times 30.0$ mm and mounted on a single cantilever clamp. The mechanical properties were measured under nitrogen in step mode every 10 °C from -50 to +200 °C. Prior to each measurement, the environment was kept at the set temperature for 10 min to ensure thermal equilibration.

Tether Structure Investigation. Model Curing Studies. The curing behavior of the epoxy/amine mixtures without the core silsesquioxane was examined using pure 4-vinyl-1,2-cyclohexene epoxide/DDM. The same variable N as in OC/DDM composite formulations was used. 4-vinyl-1,2-cyclohexene epoxide (1.0 g, 5 mmol) and varying amounts of DDM were kept at 150 °C under N_2 for 10 h. Products were viscous liquids and readily soluble in common solvents, e.g., acetone and chloroform. The disappearance of epoxy rings in the allyl glycidyl ether/DDM mixture during reaction curing was monitored by 1H NMR. Typical epoxide ring 1H signals at δ 3.14, 2.79, and 2.59 were monitored in $CDCl_3$ solution. These model materials are also used as standards in the tether structure studies below.

Direct Analysis of Organic Tether Structure by GPC. Nanocomposite organic tethers were isolated by dissolving the silica core with HF and extracting the organic components for GPC analysis. Reference GPC chromatograms were generated using the model compounds prepared above. These products contain ideal tethers without inorganic components (spacer groups), and GPC data can be used to identify peaks in the HF-derived tether GPC chromatograms.

Various OC/DDM composites were ground into powders and 50 mg of each powder were suspended in 3 mL of THF in a polyethylene bottle. HF, 50 μ L (50%), was added to the solution, and the mixture was kept at room temperature for 2 days. THF and HF were removed with vacuum-drying. The residual material was mixed with freshly dried THF to extract the organic components. Since grinding OC/DDM provided a mixture of fine and coarse powder, and the coarsest powders required more than 2 days of digestion, the powders remaining after 2 days were removed by filtration before GPC analysis. In a previous study,⁴⁵ we found that HF has no effect on the stability of the tether fragments released during digestion. In GPC analysis, signals were recorded using a UV detector. Elution times for all peaks were compared with reference GPC peaks and properly assigned.

Dynamic Molecular Simulation. Molecular modeling studies were conducted using the Insight II (Molecular Simulations Inc., San Diego, CA) molecular modeling package on a Silicon Graphics Octane platform. The structures of the OG and OC monomers were first minimized with the steepest gradient method with 1000 iterations. The monomers were then duplicated and two identical monomers were connected with two tethers; two arms at diagonal positions on one face of the monomer were linked to the opposing two diagonal arms of the second monomer through DDM. These dimer structures were again minimized with the same steepest gradient method followed by the conjugate gradients method for a total of 1000 iterations.

The molecular dynamics (MD) simulation was then continued using the DISCOVER module of Insight II with a CVFF force field. It was performed with 1 fsec time interval at 423

K (150 °C) for 10 ps in a vacuum. After MD simulation, the potential energy profile was checked to make sure that the system was in equilibrium.

X-ray Diffraction (XRD). OC monomer and OC/DDM nanocomposites were characterized by XRD using a Rigaku rotating anode goniometer (Rigaku Denki Co. Ltd., Tokyo, Japan). The working voltage and current were 49 kV and 100 mA, respectively. Cu $K\alpha$ ($\lambda = 1.54$ Å) radiation with a Ni filter was used. OC powder was mounted and pressed on a glass holder and scanned from 2 to 40° in increments of 0.2°. OC/DDM nanocomposites were mounted on an aluminum holder and scanned following the same methods for OC monomer. Bragg's law was used to calculate the d spacings.

Transmission Electron Microscopy (TEM). Nanocomposite structure was imaged using a JEOL 400 EX high-resolution electron microscope to observe potential nanosized phase segregation. OC/DDM ($N = 1.0$) was cut into a small pillar-shaped piece and microtomed using a diamond knife. A thin section (50 nm thick) was placed on a sample grid (SPI Inc.) and carbon coated. TEM images were then taken at 400 kV without staining.

Results and Discussion

In our recent OG/DDM nanocomposite studies,²⁹ the network architecture and the macroscopic mechanical properties were characterized providing initial data for structure–property relationship studies in a chemically well-defined nanocomposite system. Related nanocomposites are accessible simply by modifying the epoxy tether structure only. For example, octa(ethylcyclohexylepoxidedimethylsiloxy) silsesquioxane (OC) differs only slightly from OG as discussed below. Thus, all cure conditions being equal, investigation of the OC/DDM nanocomposite macroscopic properties should provide comparative structure–property relationships that emphasize these differences.

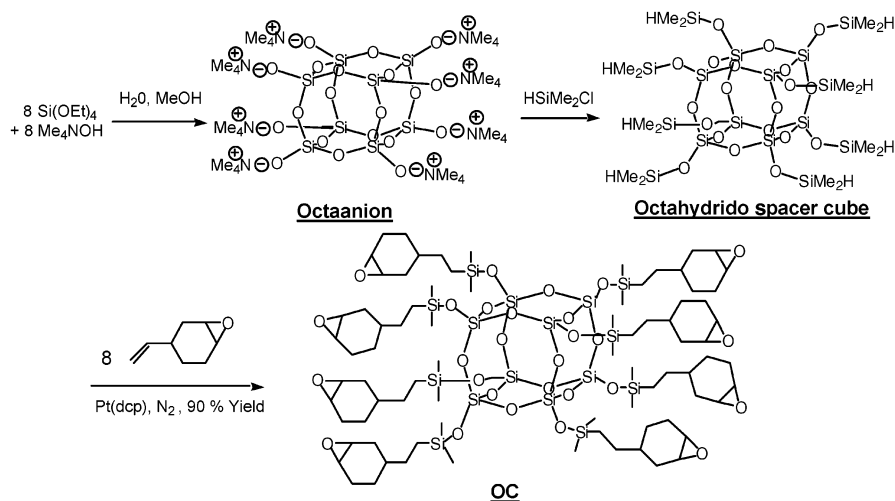
In the following sections, we first compare the OC/OG monomers and then discuss the unique cure behavior of OC/DDM system. This is followed by sections on characterization of the OC monomer and OC/DDM nanocomposites using FTIR, TGA, and DSC. Nanocomposite mechanical behavior, as determined using DMA and tensile/fracture tests, is then examined. Then, simulation studies were run to correlate tether segmental motions with observed mechanical properties. The next section explores a new nanocomposite that combines the best features of both materials. Model curing studies are also discussed. Finally, the TEM characterization of OC/DDM nanocomposite morphology is reported.

OC/OG Monomer Comparison. The OC monomer was synthesized (Scheme 2) as discussed in the Experimental Section. Its structure and purity were confirmed by 1H NMR and GPC. Because the synthesis is similar to that of OG,^{29,33} details are not discussed here. One physical difference is that OC is a solid (mp ~ 125 °C) while OG is a liquid at room temperature. However, melts of both materials can be processed equally easily at 150 °C, the curing temperature used in this study.

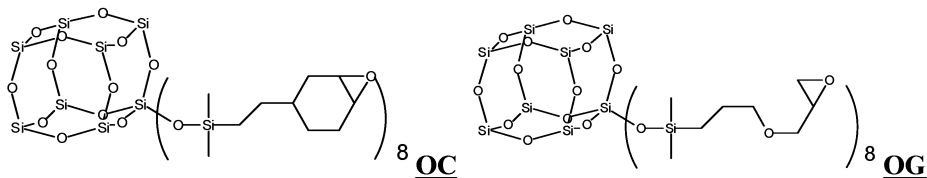
Comparison of OC with OG shows that (1) the epoxy ring tethers both have eight atoms, (2) the sixth chain atom in OC is a CH_2 vs O in OG, and (3) OC has one extra CH_2 that forms a ring, whereas OG is linear. In essence, they differ by one CH_2 and a ring. Scheme 3 illustrates the tether molecular structures of OC and OG.

OC/DDM Curing Behavior. The incorporation of the cyclohexyl ring into the epoxy tether structure changes the cure mechanism significantly in comparison

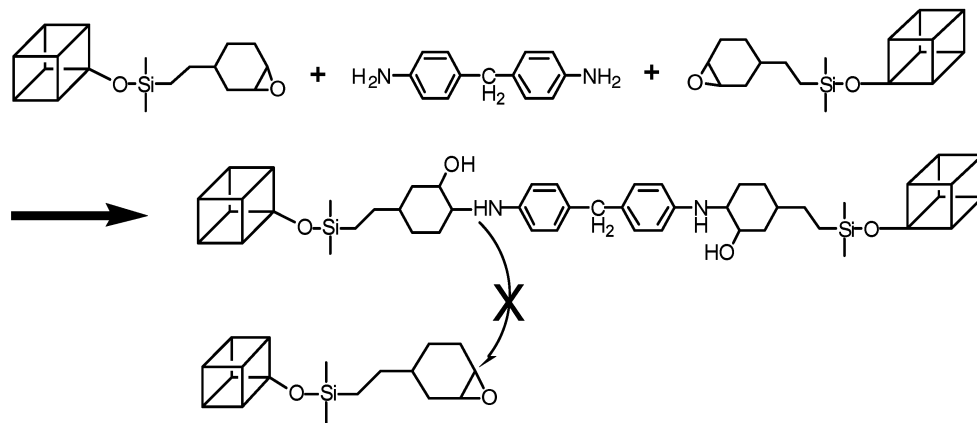
Scheme 2. OC Synthesis Steps



Scheme 3. Comparison of the OC and OG Tether Structures



Scheme 4. Formation of an Epoxy Nanocomposite with Completely Linear Tethers



with OG curing. The ring structure introduces considerable steric rigidity that can be expected to hinder the approach of the amine group to the epoxide. This is particularly evident once an amine group has already reacted with an epoxide. In this instance, reaction with a second epoxide does not occur, as demonstrated below. In contrast, for OG, two epoxides can react with one NH_2 group to form doubly bridging or bifurcated tethers (two to four cube vertices per tether).²⁹ Another factor that contributes to lower reactivity is that the increased rigidity of the cyclohexyl tethers can be expected to reduce the effective reaction volume. As a result, only linear tethers are likely to form between two cubes and the tether architecture will be significantly simpler than in the OG/DDM system. Thus, the maximum cross-link density with minimum structural defects should result when equal amounts of epoxide and amine groups are mixed, $N = 1$. Scheme 4 illustrates linear tether formation for cyclohexyl epoxy functionalized cubes.

When the stoichiometry is not $N = 1.0$, pendant unreacted moieties (defects) must result, their types

depending on the stoichiometry. At $N < 1.0$, unreacted OC groups remain, whereas at $N > 1$ with excess DDM, longer pendant groups consisting of one OC and one DDM are likely to form. Even free DDM may exist. At $N = 1.0$, linear tethers will dominate the network structure. In real networks, all of these structures may exist at the same time. Nevertheless, these three cases are thought to represent the three main nanoarchitectures that can be found in OC/DDM nanocomposites. Concrete evidence that supports this is presented below. Scheme 5 illustrates these three major networks with representative stoichiometry.

For the OG/DDM system, we know from GPC studies that the majority of the tethers are linear at $N = 1.0$. Therefore, comparison of the two systems is best made at $N = 1.0$ where the tether architecture is most uniform, as is the cross-link density.

DRIFT spectroscopy was used to monitor curing in OC/DDM mixtures and to confirm the preservation of the cube structure. Figure 1 shows DRIFT spectra of OC/DDM nanocomposites with various N s. The spectra

Scheme 5. Possible Network Structures in OC/DDM Nanocomposite at Various Stoichiometries

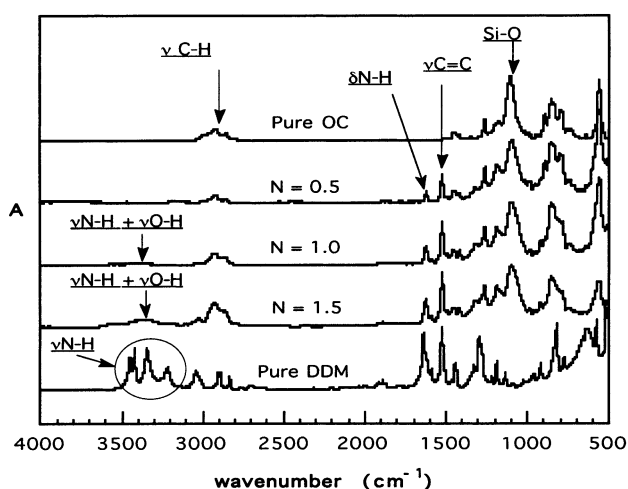
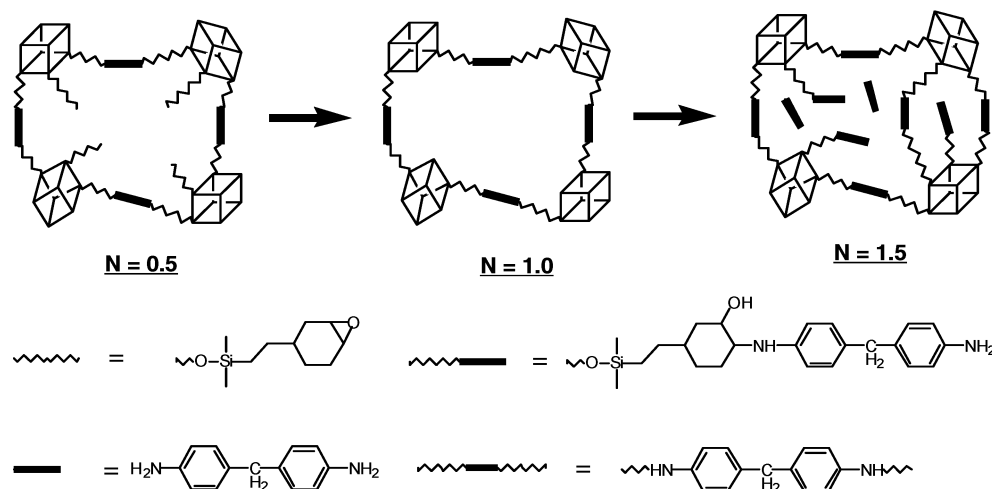


Figure 1. DRIFT spectra for selected OC/DDM nanocomposites and the reactants.

of pure OC monomer and DDM are included for comparison. These spectra were normalized to the strong cage $\nu(\text{Si-O})$ at $\sim 1100 \text{ cm}^{-1}$, used as an internal standard. The presence of this peak^{46,47} in all of the spectra indicates that the cube structure is not perturbed by processing. A degraded cube structure would produce broad asymmetric peaks.⁴⁷⁻⁴⁹ Table 4 summarizes characteristic IR absorption peaks for epoxies and silsesquioxanes.⁴⁹⁻⁵⁰

Some changes in peak patterns are observed with varying formulations upon curing. The symmetric/asymmetric $\nu(\text{N-H})$ peaks appear strongly at $3300\text{--}3500 \text{ cm}^{-1}$ in pure DDM. They disappear almost completely in the nanocomposite spectra except at $N=1.5$. The $\delta_s(\text{N-H})$ band at 1617 cm^{-1} is also strong, but diminishes as OC loading increases due primarily to dilution. The $\delta_s(\text{N-H})$ peak decreases faster than the $\nu_s(\text{C=C})$ peak as N-H bonds react with epoxy groups while C=C bonds remain but are diluted during curing. The intensity of the aliphatic $\nu_s(\text{C-H})$ at $2800\text{--}3000 \text{ cm}^{-1}$ remains unchanged during curing.

DSC and TGA of OC. The thermal behavior of the OG and OC monomers characterized by DSC and TGA are compared in Figures 2 and 3, respectively. OC melts at $\sim 125 \text{ }^\circ\text{C}$ (endotherm in DSC) and begins to decompose at $\sim 400 \text{ }^\circ\text{C}$. The char yield in N_2 is higher for OG because of its relatively higher silica content. The OC

Table 4. Characteristic Absorptions of Epoxy and Siloxane Functional Groups^{49,50}

functional group	wavenumber (cm^{-1})	vibration type ^a
Si-H	~ 2200	ν_s
Si-H	$800\text{--}950$	δ_s
Si-O-Si	$1030\text{--}1110$	ν_s
N-H	$1580\text{--}1650$	δ_s
N-H	$3400\text{--}3500$	$\nu_s, \nu_{as}, \text{doublets}$
C-N	$1250\text{--}1360$	ν_s
O-H	$3200\text{--}3500$	ν_s
C-H, aliphatic	$2840\text{--}3000$	ν_s, ν_{as}
C-H, aliphatic	$1370\text{--}1450$	δ_s
C-H, aliphatic	$1150\text{--}1350$	ω, τ
C-H, aromatic	$3000\text{--}3100$	ν_s
C-H, aromatic	$675\text{--}900$	out-of-plane bending
C-H, aromatic	$1000\text{--}1300$	in-plane bending
C=C, aromatic	$1400\text{--}1500,$ $1580\text{--}1600$	ν_s
	1250	ν_s
	$810\text{--}950$	ν_{as}
	$750\text{--}840$	$\nu_s, 12 \mu \text{ band}$
C-H in	$2990\text{--}3050$	ν_s

^a ν_s : symmetric vibration. ν_{as} : asymmetric vibration. δ_s : in-plane bending (scissoring). ω : out-of-plane bending (wagging). τ : out-of-plane bending (twisting).

ceramic yield in air was 46.7% vs 47.8% theory. For both OG and OC, the measured ceramic yields are slightly lower than the theoretical values (48.3% vs theoretical 49.7% for OG) possibly because of partial sublimation as seen for some cubes studied earlier.^{30,33-36}

However, in both DSC and TGA plots, it is clear that OC is more stable than OG; the 5% mass loss temperature for OC is higher than OG by $\sim 50 \text{ }^\circ\text{C}$ and the main decomposition temperature is also higher accordingly. The presence of cyclohexyl groups in OC affords additional thermal stability despite the relatively low silica content. Additionally, in the DSC, a small exotherm appears for OC at $350\text{--}400 \text{ }^\circ\text{C}$ suggesting self-polymerization at these temperatures, where decomposition is already dominant for OG. When OC was heated at $\sim 350 \text{ }^\circ\text{C}$ for several hours under N_2 , in a separate test, it forms a solid, probably via ring-opening polymerization.

Thermal Gravimetric Analysis (TGA) of OC/DDM Nanocomposites. Figure 4 shows TGA plots of

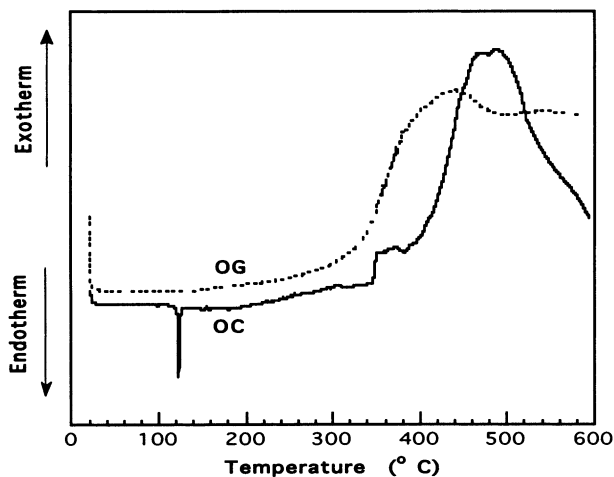


Figure 2. DSCs of OG and OC cube. (5 °C/min/N₂, first run).

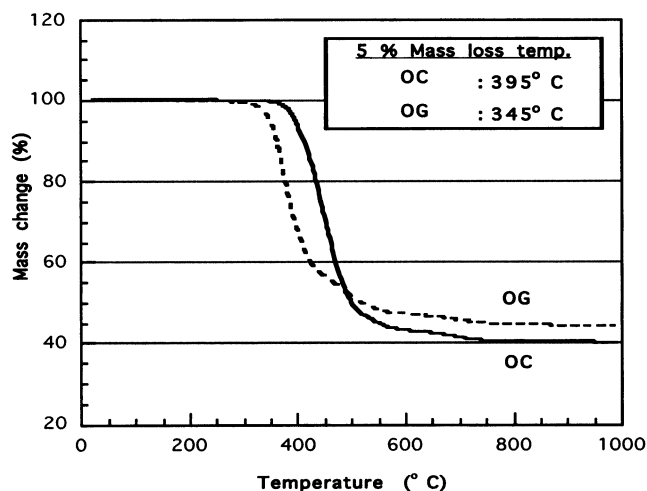


Figure 3. TGAs of OG and OC cube. (5 °C/min/N₂).

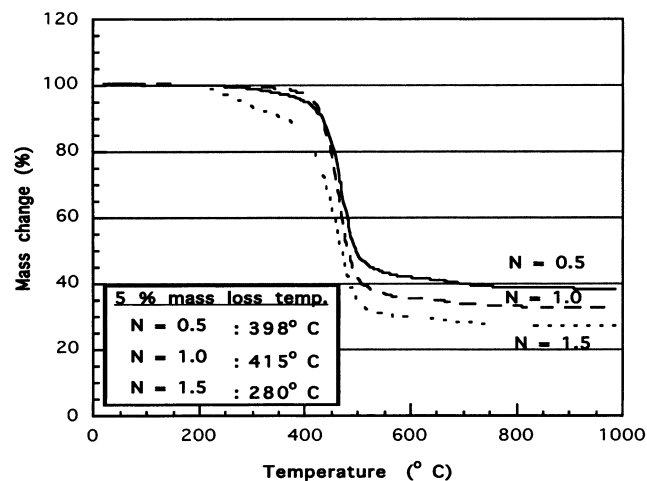


Figure 4. TGA data for selected OC/DDM nanocomposites.

OC/DDM nanocomposites with three different N s. These three composites represent the three general network types displayed in Scheme 4.

Although the char yield is highest for $N = 0.5$ because the silica content is highest, the best 5% mass loss temperature is obtained at $N = 1$ where the cross-link density is highest and the number of pendant groups or defects is lowest. In comparing $N = 0.5$ and 1.5 where pendant groups form with excess epoxide and DDM

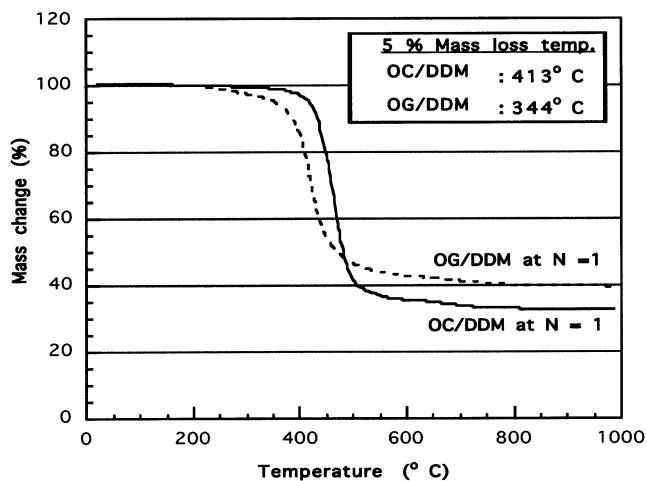


Figure 5. Comparison of the 5% mass loss temperatures OG/DDM with OC/DDM at $N = 1$.

respectively, decomposition occurs at temperatures <400 °C.

As expected, mass loss is much greater for $N = 1.5$ because the pendant groups are OC/DDM units rather than just OC units at $N = 0.5$. The 5% mass loss temperatures are ~280 vs ~400 °C for $N = 0.5$. Pure DDM undergoes complete mass loss at ~250 °C. The HF core dissolution studies below indicate traces of free (unreacted) DDM at $N = 1.5$. Overall, these results suggest that the initial mass loss at $N = 1.5$ is due to the decomposition of DDM terminated pendant groups and some free DDM. The primary decomposition temperatures for all three nanocomposites are consistently at ~450 °C.

Comparison of TGA results for OG/DDM and OC/DDM, at $N = 1.0$ (Figure 5) shows that OC/DDM is more stable than OG/DDM. Both 5 and 40% mass loss temperatures are higher for OC/DDM by approximately 70 and 50 °C, respectively. These increased thermal stabilities are most likely due to the cyclohexyl ring in OC/DDM tethers vs linear OG/DDM tethers with ether links. Similar improvement in thermal stability is seen for organic polymers that incorporate cycloaliphatic groups in flexible aliphatic chains.^{51–54}

As with typical epoxy resins, optimal thermal stabilities for cube nanocomposites are obtained by minimizing network defects and increasing cross-link densities. In traditional organic epoxy resins the highest cross-link densities are normally obtained at $N = 0.5$. For example, the thermal stabilities of the diglycidyl ether of bisphenol A (DGEBA) cured with DDM^{29,55} or phenylenediamine (PDA)⁵⁶ are highest at $N = 0.5$ where the cross-link densities are highest and presumably the number of defects is at a minimum.

If the silica core represents a “constant in the equation that defines nanocomposite properties,” and is in fact the smallest single particle of crystalline silica, then the tethers must represent the variables in this equation. Thus, it is not surprising that the thermochemical behavior of the nanocomposites is determined by the tether architecture and thermal stability properties given that the cubic core is in fact rigid and inorganic. Likewise, the mechanical properties studies are dominated by tether architecture.

Dynamic Mechanical Analysis (DMA) and Tensile and Fracture Testing of Nanocomposites. Figures 6 and 7 show the storage moduli and $\tan \delta$

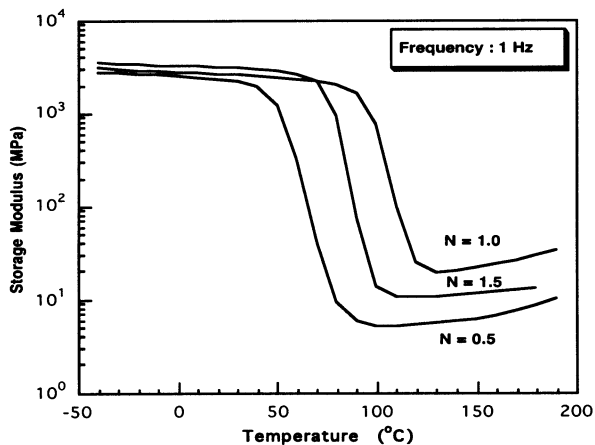


Figure 6. DMA storage moduli for selected OC/DDM nanocomposites.

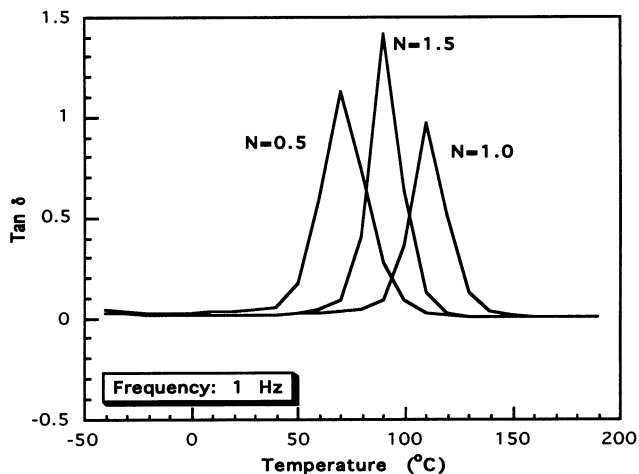


Figure 7. DMA tan δ data for selected OC/DDM nanocomposites.

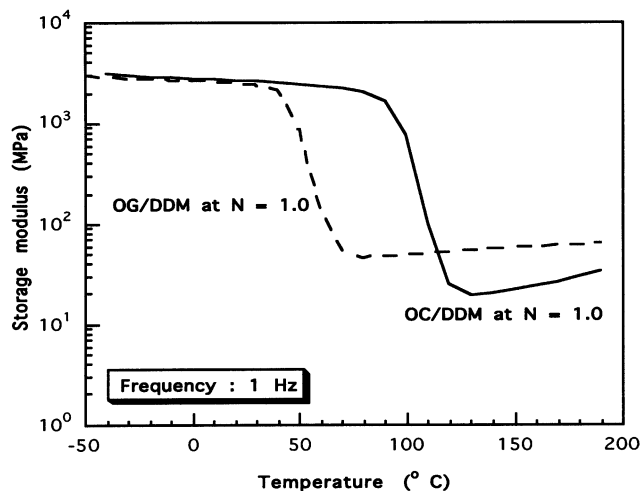


Figure 8. DMA storage moduli for OG and OC/DDM nanocomposites at $N = 1$.

profiles for OC/DDM at three N s. In these profiles, the glass transition temperatures and rubbery state moduli provide information about cross-link densities that can be used to further understand the nano architectures. As noted above, the global properties of OG/DDM and OC/DDM are best compared at $N = 1$; thus, Figures 8 and 9 compare storage moduli and tan δ of OC/DDM and OG/DDM at $N = 1.0$. Figures 10 and 11 plot tensile

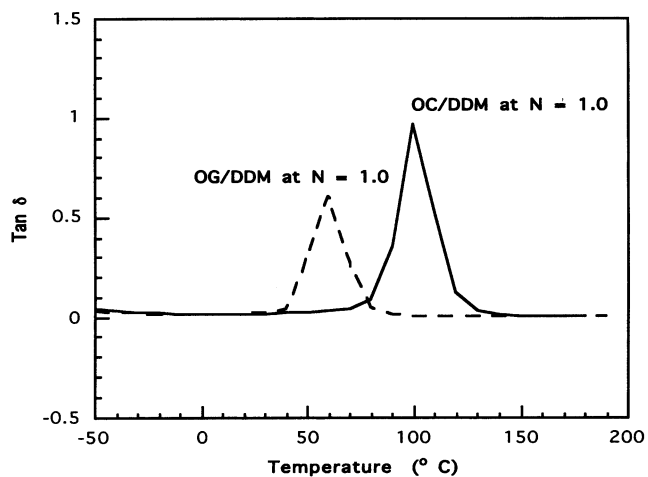


Figure 9. DMA tan δ 's for OG and OC/DDM nanocomposites at $N = 1$.

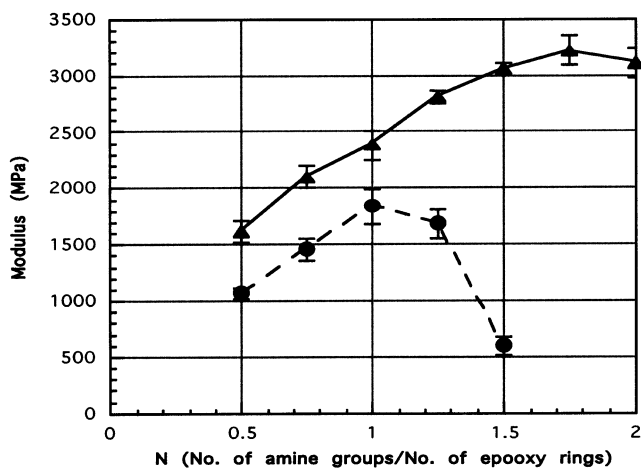


Figure 10. Elastic moduli of OG and OC/DDM nanocomposites at various N s.

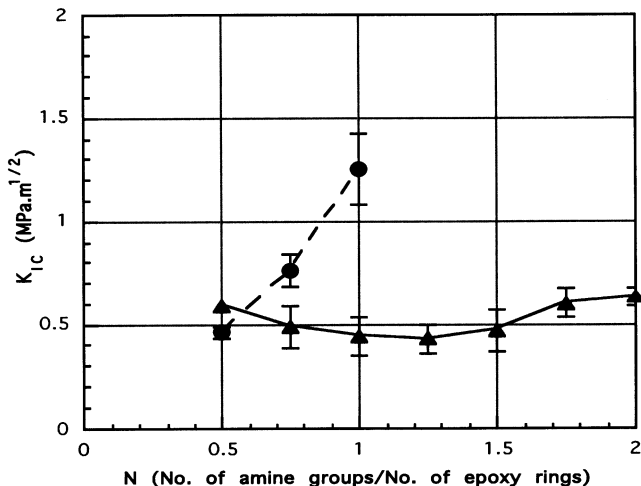


Figure 11. Fracture toughness data for OG and OC/DDM nanocomposites at various N s.

and fracture toughness data for OC/DDM and OG/DDM nanocomposites at room temperature as a function of N . Each data point is an average of at least five measurements.

Table 5, provides a summary of selected mechanical properties from Figures 7–11 and data on DGEBA/DDM (DEGBA MW \approx 340), a typical epoxy resin. The literature suggests that typical epoxy resins exhibit

Table 5. Selected Mechanical Properties of OG, OC, and DGEBA/DDM Resins^{28,29}

material	T_g at $N = 0.5$ (1.0), °C	storage moduli $N = 0.5$ (1.0), GPa	elastic moduli $N = 0.5$ (1.0), GPa	K_{Ic} at $N = 0.5$ (1.0), MPa m ^{0.5}
DGEBA/DDM	160 (\approx 100)	2.0 (2.0)	2.0 (2.4)	0.8 (1.3)
OG/DDM	- (60)	0.9 (2.0)	1.1 (1.8)	0.5 (1.2)
OC/DDM	60 (100)	1.5 (1.8)	1.6 (2.4)	0.6 (0.4)

their highest T_g 's and rubbery state moduli at $N = 0.5$ where cross-link densities are highest and defects are minimal.^{40–44} Surprisingly we find that all of the systems we have studied, including DGEBA/DDM, exhibit their highest elastic moduli and fracture toughness at $N = 1$.

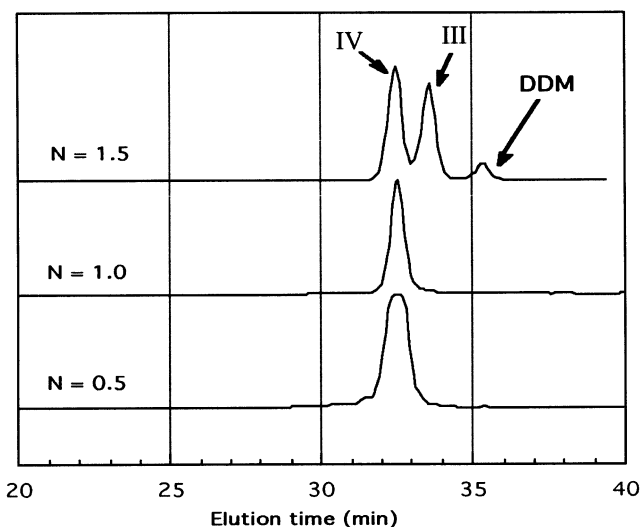
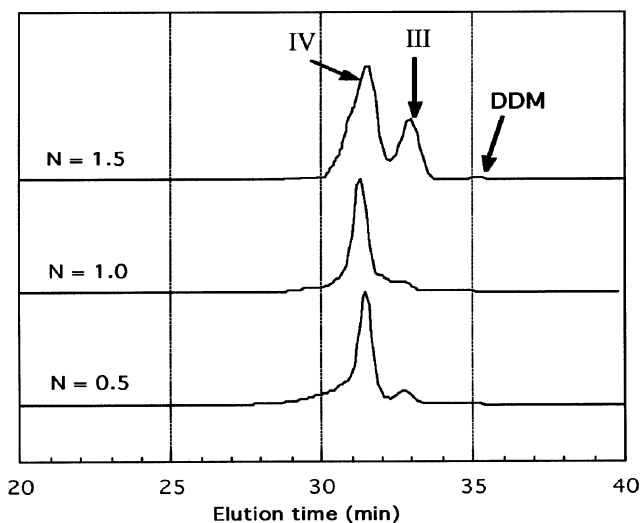
The DGEBA/DDM system has a higher T_g at $N = 0.5$ whereas the OG/DDM system has none. Both of these epoxies have their highest cross-link densities at $N = 0.5$ because the cure chemistry allows formation of bifurcated tethers as discussed below.

In contrast, the OC/DDM composites have their highest T_g 's and rubbery state moduli at $N = 1.0$ (Figures 6 and 7), suggesting a maximum in cross-link density, as demonstrated below. This result provides collateral proof that the bulky cyclohexyl rings hinder reaction of a second epoxy at the amine such that only linear tethers form under all reaction conditions (see below). In addition, at $N > 1$ the elastic modulus increases to as high as 3.3 GPa at $N = 1.5$. This is a very unusual result. Given that our target nanocomposite designs should lead to completely discontinuous nanocomposites wherein load transfer must be from tether to cube and back again, tether structure and behavior must be responsible for all of the observed properties. Before we discuss the effects of tether structure and behavior in OG/, OC/ and DGEBA/DDM resins, it is pertinent to prove, as we did for OG/DDM, that the OC/DDM nanocomposites are homogeneous.

Homogeneity in OC/DDM. Homogeneity was determined in several ways, first by modeling the cure reactions, then by dissolution of the silica core with HF followed by GPC analysis and comparison with the model curing reaction products, and finally by TEM micrographs.

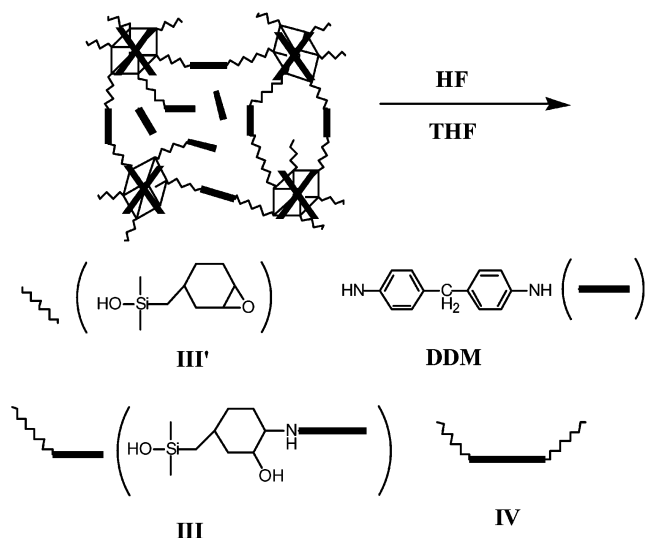
Cure Modeling Study. Because the nanocomposite resins are insoluble, conventional solution ¹H NMR or GPC analytical techniques cannot be used. Thus, the curing chemistry at various N s was modeled using 4-vinyl-1,2-cyclohexene epoxide in place of OC, using the standard curing conditions. The resulting products remain soluble and amenable to analysis by GPC and solution ¹H NMR.

¹H NMR and GPC (Figure 12) show that all the epoxy groups react at 150 °C at $N \geq 1$ but unreacted epoxy groups remain at $N \leq 1.0$. Since cross-linking does not limit the cure reaction, these results suggest that for OC/DDM nanocomposites, DDM act as a difunctional curing agent. The likely explanation is that discussed above; i.e., the bulky cyclohexyl ring inhibits secondary amine curing reactions. Therefore, OC/DDM nanocomposites contain only linear tethers and maximum cross-link densities obtain only at $N = 1.0$. This observation is contradictory to the conventional notion that DDM is a tetrafunctional cross-linker.^{40–43,57} For the OG/DDM nanocomposite, DDM does indeed offer tetrafunctional behavior.²⁹ Unfortunately, the exact distributions of tether structures (linear vs defect) are hard to assess

**Figure 12.** GPC traces of the model curing reactions at three N s. See Scheme 6.**Figure 13.** GPC traces of THF extraction of HF hydrolyzed OC/DDM at three N s. See Scheme 6.

quantitatively using model studies only. Fortunately, they can be estimated using means discussed in the next section.

Direct Tether Structure Studies. Concrete evidence for tether architecture was obtained by HF dissolution of the silica core followed by THF extraction and GPC analysis of the organic tether fragments that remain (Figure 13). In related studies, it was shown that organic fragments are not affected by HF under the conditions used.⁴⁵ When the products from the model curing studies and the extracted tethers are compared in GPC analysis, each peak can be assigned properly and the tether structures can be determined. Possible tether and pendant group structures are illustrated in Scheme 6. Figure 12 shows the GPC trace for the model curing studies discussed above. Three peaks are observed. First, free DDM appears at 35.5 min elution time. Then, peaks at 32.5 and 33.5 min are thought to be **IV** and **III**, respectively. Although only a single peak for **IV** appears for both $N = 0.5$ and $N = 1.0$, this result suggests different network structures for each case. At $N = 0.5$, excess epoxy groups guarantee the formation of **IV**. At the same time, some unreacted epoxide (**III**) should be seen in the GPC. However, the absence of any

Scheme 6. Possible Tether and Pendant Group Structures of OC/DDM^a

^a Key: (III') unreacted epoxide; (III) pendant group with DDM; (IV) linear tether; (DDM) free DDM.

extensive conjugation makes detection of III' by UV absorption more difficult than III, IV, and free DDM. GPC analysis with an RI detector was even worse giving very small and inconsistent peak intensities. This study assumes that III' exists at $N = 0.5$ although it is not detectable. However, the same single peak for $N = 1.0$ indicates the formation of different reaction products. Because equal amounts of epoxide and amine groups were mixed, incomplete reaction would generate III', III, or free DDM. However only a single peak at $N = 1.0$ indicates that all of epoxide and amine reacted to form IV. Moreover, all possible peaks for III, IV, and free DDM appear at the same time when excess DDM is used ($N = 1.5$).

A similar pattern is observed for HF-generated tethers extracted using THF. The notable difference is that all the peaks were shifted toward the higher molecular weight region (lower elution time). III and IV appear at 33.0 and 31.5 min respectively. This is because the tethers contain dimethylsiloxy end groups, thus increasing the effective hydrodynamic volumes. Additionally, a peak for residual III at 33.0 min is observed at both $N = 0.5$ and $N = 1.0$ probably because the increased viscosity from cross-linking hinders complete reaction. For $N = 0.5$, tether IV must coexist with some III' and III. Note that the III' peak is not observed for the same reason as in the model cure studies. For $N = 1.0$, tether IV is the dominant nanoarchitecture with a trace amount of III' and III, whereas III, IV, and free DDM peaks all appear for $N = 1.5$. These results provide a clear understanding of network structure and support our argument that only linear tethers form in the OC/DDM cure reaction because of the steric hindrance of bulky cyclohexyl group.

Transmission Electron Microscopy. The above results suggest that the components in OC/DDM are uniformly distributed at the nanometer scale (1–5 nm) and their nanoarchitectures are well-defined. However, it is not clear if OC/DDM is homogeneous at larger length scales, e.g., 10–100 nm. Therefore, the $N = 1$ OC/DDM nanocomposite was characterized by TEM to search for possible phase segregation. The sample was not stained because the electron density differences

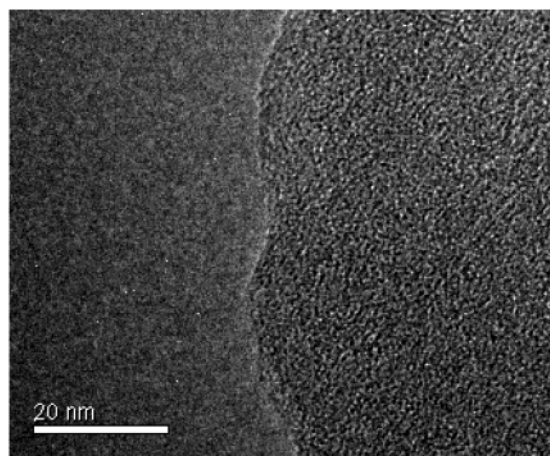


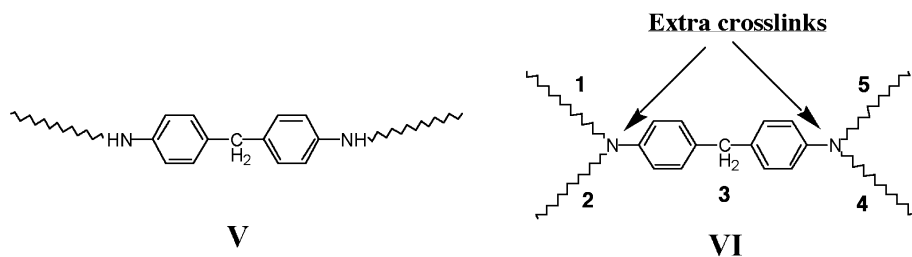
Figure 14. High-resolution TEM of OC/DDM ($N = 1$) embedded in epoxy support (left half of the image).

between the core and the organic tethers should produce sufficient contrast to observe any significant phase segregation. Figure 14 is a high-resolution TEM image of OC/DDM at $N = 1.0$. In this image, no phase segregation is observed even at nanometer length scales. Electron beam damage to the sample must be considered in understanding these results. High electron doses in high-resolution TEM can severely damage polymer links producing replicas of the original nanostructure.⁵⁸ Nevertheless, electron density differences between the core and potentially damaged organic components would still be large. The theoretical size of the cube core is ~ 1 nm including spacer groups and 1.5–2.0 nm including tethers.³³ If a few cubes formed clusters, their sizes would easily reach 5–10 nm and should be visible in Figure 14. There is no evidence that this occurs.

These results suggest that cubes and tethers are uniformly distributed at the nanometer length scale because, despite their different electron densities, no electron density contrast was discerned. Again this suggests that the nanocomposites are likely homogeneous.

Structure-Processing Property Relationships. Segmental Architecture. Understanding the above property differences may be key to developing structure–processing–property relationships in epoxy nanocomposites. The first step is to understand what tether structures form. Scheme 5 illustrates the two types of reaction derived defect structures possible in epoxy resins. Scheme 7 illustrates two tether structures that generate “minimum defect” networks likely to lead to optimal properties.

At $N = 1$, the linear tether segments V that join two cube vertices are expected to predominate based on curing chemistry stoichiometry. OC/DDM single tether segments have average MWs nearly identical with single OG/DDM tethers (597 vs 577 g/mol). At $N = 0.5$, the OG/ and DEGBA/DDM resins form bifurcated tethers. In OG/DDM, these bifurcated tethers consist of five segments with two cross-links connecting four cube vertices (VI). The average MW of these segments is 20% of a single tether MW. Cross-link densities are about 1.5 times higher for OG/DDM at $N = 0.5$ ($\sim 4.4 \times 10^{-3}$ mol/cm³) than for OC/DDM at $N = 1$ ($\sim 2.9 \times 10^{-3}$ mol/cm³).⁵⁹ In comparison, DGEBA/DDM has an average segmental MW of 474 g/mol and a cross-link density of 2.11×10^3 mol/cm³.⁵⁹

Scheme 7. Illustration of Linear (V) and Bifurcated (VI) Tethers^a

^a For VI, five segments are connected via two cross-links to form bifurcated tethers connecting four vertices. For V, only one segment connects two vertices.

Segmental Motion. In the above, we discussed the importance of segmental architecture on thermal stabilities. Here we consider segmental motion, i.e., more degrees of freedom that evidence themselves at T_g , as perhaps ductile deformation, and its possible role in mechanical properties. If we accept the notion that the silica core is a constant for both the OG and OC nanocomposites, and use the DGEBA/DDM system as a reference baseline (DGEBA MW \approx 340), we can make some general comments about the mechanical properties of the nanocomposites studied in this work.

It is well-known that highly cross-linked systems are very brittle and are characterized by having high elastic moduli and poor fracture toughness. The mechanical properties of epoxy resin systems are normally studied at $N = 0.5$; however in our studies we focused primarily on the $N = 1$ materials. This is because $N = 1$ materials are mandated by our need to study tethers which are completely decoupled from each other to fully understand transfer of mechanical load in completely discontinuous nanocomposites.^{28–29,31} The results of these studies provide new perspectives in epoxy resin chemistry and on nanocomposite properties.

The conventional DGEBA (MW \approx 340)/DDM system ($N = 0.5$), with a Young's modulus of \approx 2 GPa and a fracture toughness of $0.8 \text{ MPa m}^{1/2}$, can be characterized as a relatively brittle material.^{40–44} It has a reasonably high T_g (170 °C) indicating that segmental mobility is limited by the high cross-link densities and possibly the segmental architectures. Surprisingly, at $N = 1$, the Young's modulus is the same but the fracture toughness is much higher. Although the T_g drops to \approx 100 °C, this is not likely to affect the room-temperature mechanical properties. The addition of hard, reinforcing particles can be expected (see below) to increase the modulus while possibly reducing the fracture toughness.

The OG/DDM system replaces the linear, difunctional aromatic unit of the DGEBA with a rigid three-dimensional unit that uses the same reactive epoxy group but is octafunctional and roughly the same size as the aromatic core or slightly smaller. Thus, the average cross-link density is higher than in the DGEBA/DDM system, especially for the $N = 0.5$. Contrary to what might be expected for a more brittle epoxy; looking at Table 5, the elastic modulus at 1.1 GPa is only 55% of that of the DGEBA material. The fracture toughness at $0.5 \text{ MPa m}^{1/2}$ is only 60% of that of the DGEBA system. Furthermore, no T_g is observed. The latter observation indicates that segmental motion is very limited but it also may indicate that segmental motion plays a role in the observed mechanical properties. We return to this below.

In the OC/DDM nanocomposites, the $N = 0.5$ materials have high defect densities and are not considered

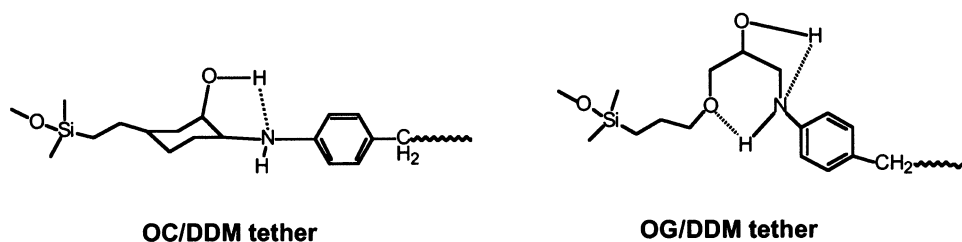
further. At $N = 1.0$, a maximum in cross-link density is reached as determined by chemical analysis above. In principle, a maximum in elastic modulus and fracture toughness should also result given the above results for the DGEBA and OG/DDM materials. In contrast, the elastic modulus continues to rise up to $N = 1.75$ from 2.0 GPa at $N = 1$ to 3.3 GPa. The fracture toughness does not change at all, staying about $0.5 \text{ MPa m}^{1/2}$ for all compositions. The T_g at $N = 1.5$ is \approx 95 °C, so the change in mechanical properties cannot be ascribed to T_g changes. These results do not seem to reflect typical epoxy resin behavior. If we return to the argument that the cube cores represent hard particles with constant properties, then we must accept that changes in properties arise from tether behavior.

We have noted before that the cube nanocomposite materials may behave like interfacial or interphase materials in macroscopic organic/inorganic composites.^{28,29} Interphase materials are proposed to exist at distances of 1–4 nm from the surface of the inorganic component as in the nanocomposites prepared here.²⁸ The organic components in the interphase are expected to behave differently from the bulk polymer.^{37,38} The question is how? If we begin by considering segmental (or tether) motion, then perhaps we can identify some general behavior patterns.

In organic polymers, even in highly cross-linked materials, segmental motion is expected to be cooperative, even through cross-links. Thus, the glass transition temperature is really where segmental motion becomes cooperative. In interphase materials,^{28,29} segmental motion will be hindered by the inorganic phase to some degree. Some cooperative motion will be available along the interface but it will be slowed by the segments immobilized by interactions with the inorganic phase. In the nanocomposites made here, the tethers represent individual segments isolated from other segments. Hence, their motion probably will be similar to those segments of polymers immobilized at the inorganic phase in the interphase.

Because cubes are immobilized by localized cross-links at vertices, they likely limit cooperative motions of multiple tethers. Consequently, macroscopic relaxation must be a combination of the relaxation motions of individual tethers. This is a very unique feature of cube nanocomposites as compared with organic thermosets and offers a rare chance to isolate and study well-defined tether segmental motions. That is, the macroscopic glass transition provides information about the relaxation of individual tether segments. Thus, the fact that the OC/DDM tethers relax at higher temperatures than OG/DDM tethers can be attributed to restricted motion of individual cyclohexyl units and not to restrictions in cooperative motions. This translates

Scheme 8. Possible Hydrogen Bonding (- -) in Tethers



directly into an increase in $T_g \sim 50$ °C for OG/DDM to ~ 110 °C for OC/DDM.

In summary, T_g and rubbery state modulus are always maximal at the highest cross-link density, but the stoichiometry for the highest cross-link density depends on the cure mechanism which in turn determines the tether architecture. DMA results suggest that linear tethers form for OC/DDM. They also suggest that individual tether relaxation motions dominate macroscopic glass transition behavior and thus nanocomposites with rigid tethers exhibit better thermomechanical stabilities.

Increases in OC Modulus. One important observation is that the OC/DDM modulus surpasses 3 GPa as N increases beyond the maximum cross-link density formulation at $N = 1$. Furthermore, it continues to increase as N approaches 2. In comparison, the OG/DDM and DEGBA/DDM moduli reach maxima at $N \sim 1.0$ and then fall significantly. Note that the maximum cross-link density for OG/DDM occurs at $N = 0.5$. Trends similar to those seen for OG/DDM are consistent with those observed for organic epoxy resins^{29,55-59} where moduli also increase as N increases beyond 0.5. For example, the DGEBA/DDM resin exhibits a maximum modulus of ~ 2.4 GPa at $N = 1$ vs ~ 2.0 GPa at $N = 0.5$. For OG/DDM, T_g 's begin to drop at $N > 1$, lowering the elastic moduli. The modulus cannot even be measured at $N > 1.5$ because the composites become rubbery, with T_g 's close to room temperature. For OC/DDM, T_g 's are always higher than room temperature for all N 's and thus are not expected to greatly influence mechanical properties tests.

These results suggest that OC/DDM networks become stiffer as cross-link density decreases with increasing DDM. In comparison, the OG/DDM network is stiffest at $N = 1$ and then softens as DDM loading increases. In both cases, the tethers are predominantly linear rather than bifurcated, thus multiple tethering modes are likely minimal. Therefore, the differences in behavior must originate from differences in tether structure.

As the cross-link density increases beyond the minimal defect stoichiometry $N = 1$, excess DDM will react with OC to form pendant groups or defects. At this point, network flexibility should increase. This should permit cyclohexyl groups within the network structure to adopt the most favorable ring conformation (e.g., chair) in contrast to the higher energy twist-chair or even boat conformations that might be forced upon the rings at the highest cross-link densities, at $N = 1$. These relaxed structures will be more linear than the constrained structures and should exhibit higher elastic moduli than structures that can relax only under tension.

Some support for this type of process can be envisioned, if one considers the types of configurations available to both the OC and OG tethers. Scheme 8 suggests the most favorable structures that might be

anticipated based on a relaxed network and hydrogen bonding.

To explain the increase in moduli at $N > 1$ in OC/DDM, we must assume that the relaxed structures are prevented from forming at higher cross-link densities which force the flexible portion of the ring to fold in on itself. XRD studies below also suggest that OC/DDM tether configurations change when DDM content increases. In comparison, intrachain hydrogen bonding (Scheme 8) can be suggested to favor tether folding in the more flexible OG/DDM system. Furthermore, for OG/DDM resins the presence of less rigid pendant groups at $N > 1$, further lowers T_g 's (e.g., ~ 40 °C at $N = 1.5$) and elastic moduli.

The different tether behaviors of OC/DDM and OG/DDM are also reflected in the fracture toughness studies. The OG/DDM K_{IC} is similar to that of OC/DDM only at $N = 0.5$ and reaches a maximum of ~ 1 MPa $m^{1/2}$ at $N = 1.0$. Beyond $N > 1.0$, OG/DDM becomes rubbery and no reliable measurements could be obtained. Increases in fracture toughness for off-stoichiometry formulations $N > 0.5$ are also commonly found for organic epoxy resins.^{29,55-59} In contrast, the change in the toughness of OC/DDM as a function of DDM content is very small, and K_{IC} stays around 0.5 MPa $m^{1/2}$ for all N 's suggesting that network cross-link density has little effect on the fracture toughness when tethers are too rigid to dissipate energy. Tether flexibilities for these nanocomposites are compared more quantitatively below.

Simulation Studies. In an effort to establish a more direct comparison of tether flexibility and determine if segmental relaxation or nanoflexibility can really represent macroscopic relaxation patterns, molecular modeling studies were conducted. In this study, two identical monomer cubes are connected by two tethers placed diagonally on each cube and the distance between two cubes is monitored when tethers move freely at a representative temperature of 150 °C where the nanocomposites are cured. In these systems, distances between two cubes are determined solely by two tether segmental motions and thus comparison of these distances can provide relative measure of tether rigidity. Figure 15 shows dimer structures OC/DDM and OG/DDM simulated and the range of motions measured in the study.

Simulation results show that OG/DDM tethers can extend to approximately 200% the length at the point of closest approach. In contrast, OC/DDM tethers extend to only 50% of the length at the point of closest approach. Given that these tethers have similar numbers of bonds, simulation indicates that the OG/DDM tether is more flexible than the OC/DDM tether and has larger segmental motions that likely dissipate more fracture energy.

These results appear to provide some explanation of the mechanical properties of both composites. The

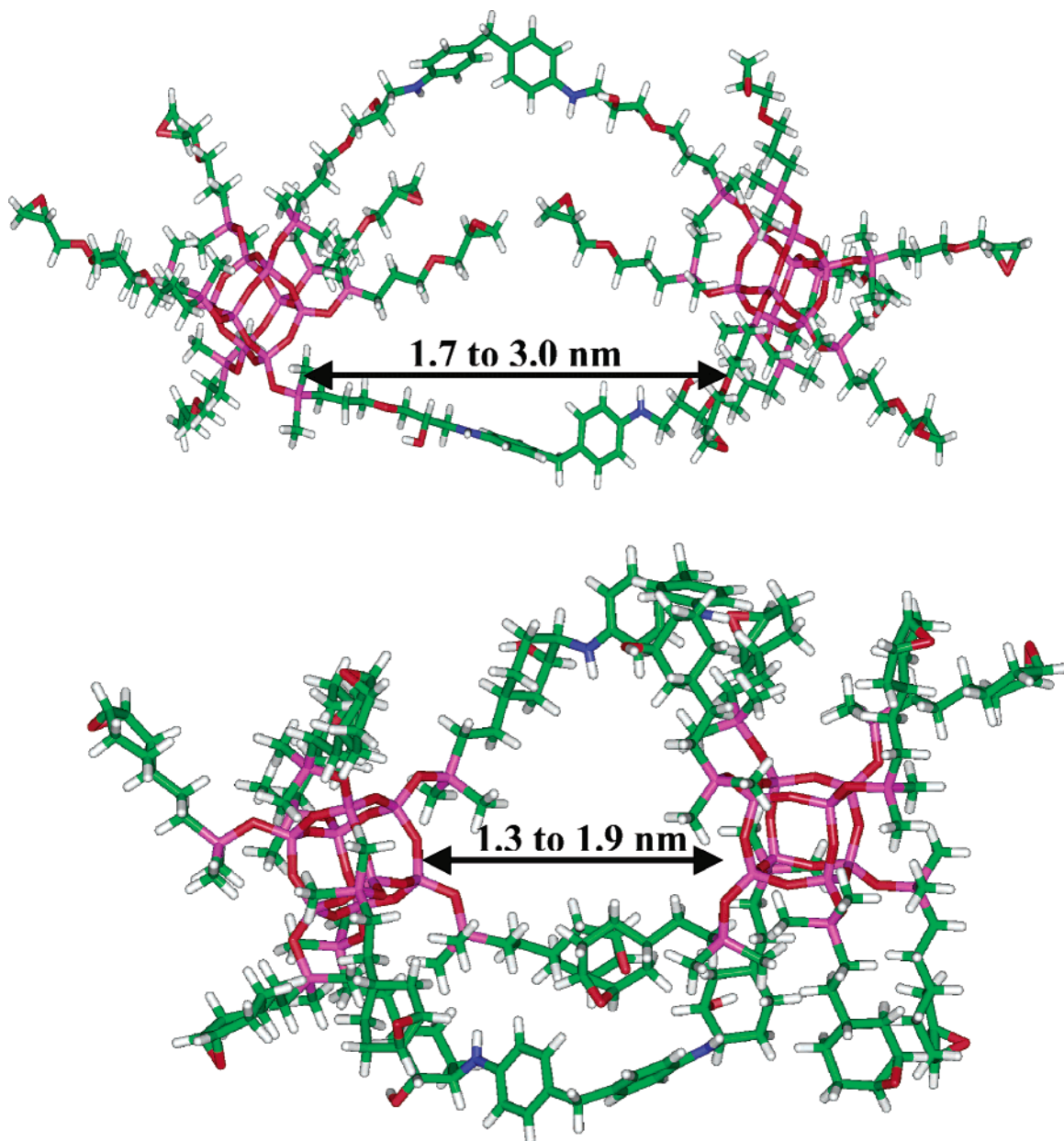


Figure 15. Cache modeling of cubes joined by two DDM/epoxy links. Molecular dynamic simulation was conducted at nanocomposites processing temperature (150 °C) and the range of motions are measured: (a) OG/DDM; (b) OC/DDM.

higher T_g and elastic modulus of OC/DDM is due to poor nanoflexibility that in turn results in poor fracture toughness. Likewise, flexible OG/DDM tethers account for lower T_g and elastic moduli and relatively higher fracture toughness. This study also suggests that investigation of tether properties and modeling their behavior can provide information about nanocomposite macroscopic behavior.

Given that both nanocomposites consist of periodic networks of well-defined single tethers and cubes, these results suggest that tether properties dominate the nanocomposite macroscopic properties. Hence, in these nanocomposites, the cubic silica core can indeed be considered a constant in the “equation” that defines materials properties. The variables in this equation are therefore the tethers and the defects.

Blending Studies. Mechanical properties tests and simulation studies suggest that modulus and fracture toughness are not likely to improve coincidentally because adjusting tether rigidity and cross-link density

in favor of one property affects the other adversely. However, given that OG/DDM is soft with a high fracture toughness and OC/DDM is stiff with a high modulus, blending OC with OG may provide both high modulus and fracture toughness. Therefore, an effort was made to combine the best features of those nanocomposites by blending.

$N = 1.25$ was selected for blending because both modulus and fracture toughness can be expected to be high. On the basis of individual moduli of 2.8 GPa for OC/DDM and 1.7 GPa for OG/DDM, the combined modulus is expected to be 2–2.5, comparable to the highest DGEBA/DDM modulus of 2.4 GPa measured earlier.²⁹ For fracture toughness, $N = 1.25$ is where K_{IC} becomes immeasurable for OG/DDM suggesting high ductility. Once K_{IC} can be measured on blending with OC/DDM, its value is likely to be high.

Thus, studies were done in which OC was mixed with OG and DDM keeping N at 1.25. The OG loading was

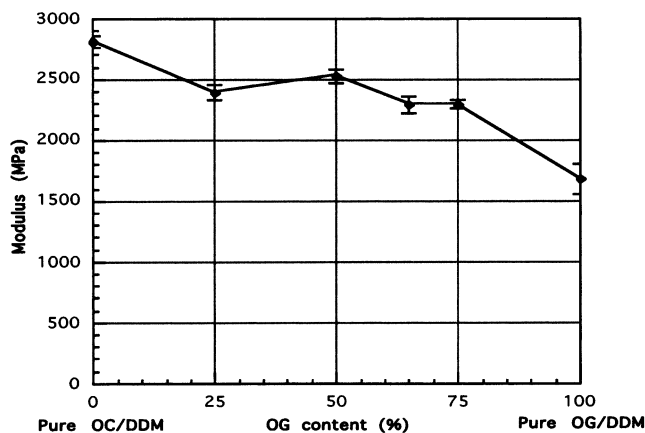


Figure 16. Tensile testing of OG/OC/DDM blends at $N = 1.25$.

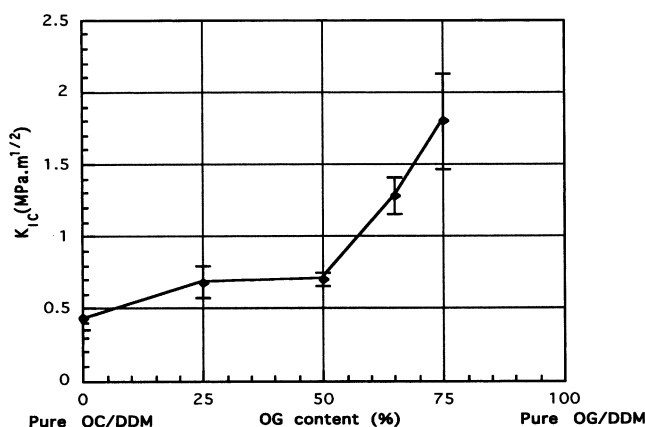


Figure 17. Fracture toughness testing of OG/OC/DDM blends at $N = 1.25$.

adjusted in increments of 25 mol %. As a result, at a composition containing 75 mol % OG, a 25% increase in elastic modulus to 2.2 GPa was observed for the blended nanocomposite with only modest improvements thereafter until pure OC is used, per Figure 16. Likewise, a large increase in the fracture toughness was observed (Figure 17) between 50 and 75 mol % OG loading. Thus, another composite with 65 mol % of OG was prepared for more careful observation. However, the maximum fracture toughness remained at 75 mol % OG. Note that in Figures 16 and 17, each data point is an average of at least five measurements.

Clearly there is a significant improvement in both properties as a result of blending. Now the important question is: "Are these results a consequence of property averaging or true tailoring of the architecture?"

The profiles in Figures 16 and 17 show distinct features that are not expected from the rule of mixtures. First, the new moduli are the median values of two composites' moduli, but they remain in the range of 2.3–2.5 GPa for all formulations, higher than values expected by the rule of mixtures. This result suggests that the rigid OC/DDM tether dominates the new elastic modulus. When networks consisting of both rigid and flexible tethers are tested under tension, network deformation is limited more by the rigid segments than the flexible ones. Thus, macroscopic stiffness depends primarily on the rigid tethers.

In contrast, fracture toughness remains around 0.7 MPa m^{1/2} until 50 mol % OG, then jumps to ~1.8 MPa m^{1/2} at 75 mol % OG. This pattern change suggests that the hypothetical K_{IC} of pure OG/DDM at $N = 1.25$ may

be above 2.5 MPa m^{1/2} if it could be measured. Thus, it appears that fracture toughness is dominated by the component with the major mass fraction; OC/DDM dominates fracture toughness until ~50 mol % OG loading, and then OG/DDM affects it more strongly at OG loadings >50 mol %. These results further suggest that each cube component and tether have different influences on the properties and some components dominate the properties on blending. Thus, the opportunity for tailoring certainly exists but simple design principles are not immediately obvious. Modeling studies should help identify some of these principles.

A discussion of possible network structures can provide some insight into the observed fracture toughness. At low OG loadings, e.g., 25 mol % OG/75 mol % OC, networks consist mostly of linear OC/DDM tethers and pendant groups. Bifurcated OG/DDM tether formation is likely limited by statistics. The probability that OG monomers are linked with each other is low due to their low concentration. Formation of hybrid tethers containing both of OG and OC units consumes some OG, further reducing the chance for OG/DDM tether formation. Thus, rigid OC/DDM tethers dominate fracture toughness at low OG loadings. At high OG loadings, e.g., 75 mol % OG/25 mol % OC, networks consist primarily of OG/DDM tethers and pendant groups. Formation of hybrid tethers reduces the chance for OC/DDM tether formation. Some bifurcated tethers also likely form due to increases in OG concentration that in turn consume more epoxide and generate more DDM terminated pendant groups. Consequently, networks consisting of more OG/DDM tethers as well as more pendant groups result in better fracture toughness.

Epoxy silica composites have also been made using sol-gel processing to create various structures including simple embedded silica particles of various sizes or interpenetrating (INP) silica networks.^{65–69} Here, condensation of alkoxysilanes and curing of epoxies proceed concurrently. Silica domain sizes can range from ~30 nm to several micrometers, usually determined by silica content (to ~30 wt %) and cure conditions. Silica particles can also be prepared separately and mixed mechanically with epoxy resins.^{70–75} Typical silica particles (~15 μ m diameter average particle size, APS) have elastic moduli of ~70 GPa, thermal expansion coefficients of 0.5 ppm/°C, and densities of ~2.2 g/cm³.⁷⁵

The thermal stabilities of silica-reinforced epoxies are usually better than pristine epoxies. Char yields (at ~900 °C) increase significantly and primary decomposition temperatures, e.g. ~50% mass loss temperatures, are also higher. For example, DGEBA/DDM reinforced with sol-gel derived silica (~10 wt %, 30 nm APS) produce 37 wt % char and exhibit 50% mass loss temperatures of ~500 °C (vs 13 wt % and ~400 °C for pristine DGEBA/DDM respectively).⁶⁸ However, epoxy these silica hybrids lose significant masses (5–10 wt %) at these temperatures <350 °C because incomplete Si-OH condensation reactions proceed further on heating beyond epoxy curing temperatures (~200 °C).

Silica incorporation also improves mechanical properties. DGEBA (Epikote 828, Shell Chemical Co. MW 390) cured with *n*-butylamine at $N = 0.5$ exhibits moduli of ~8 GPa (vs ~2.3 GPa for unfilled resin) with ~55 wt % silica loading (~30 μ m APS).⁷² Fracture toughness of this epoxy resin also improves from ~1.2 up to ~2.3 MPa m^{1/2} at the same silica loading.⁷³ Effects of silica on glass transition temperatures (T_g 's) vary greatly. For

example, the T_g of DGEBA/ethylenediamine filled with fumed silica (10 wt %, ~ 12 nm APS) remains at ~ 120 °C,⁷⁰ that of unfilled DGEBA/ ethylenediamine.⁷⁶ In comparison, T_g 's of DGEBA/tetraethylenepentamine-silica hybrid (INP structure) are eliminated completely at silica loadings >5 wt % ($T_g \sim 150$ °C for a pristine resin),⁶⁷ while T_g 's of DGEBA/dimethylbenzylamine-silica hybrids (INP) improve by only ~ 30 °C ($T_g \sim 100$ °C for pristine resin) on ~ 10 wt % silica loading.⁶⁷

In the cube nanocomposites discussed above, typical net silica loadings at $N=1$ are ~ 25 – 30 wt %. This silica is perfectly dispersed and of constant particle size, ~ 1 nm diameter. There is no clustering or even contact between particles. Thus, comparison of the properties of silica-filled epoxy systems with epoxy cube nanocomposites, while tempting, is difficult because of the many variables both in the structures of the epoxy resins, the way the silica is introduced, the curing conditions, and even the analytical techniques used.

However, some basic processing comparisons can be made. For example, epoxy resins filled with silica usually suffer from high viscosity in processing (>1000 P),⁷⁷ or the sol-gel process requires complex processing techniques. In contrast, epoxy cube nanocomposites can be readily processed like pristine organic epoxies, with no modification or viscosity issues. Char yields and thermal stabilities of cube nanocomposites are higher than those of unmodified epoxy segments used for forming tethers. In particular, initial mass losses at temperatures <350 °C are negligible. T_g 's are determined not by silica loadings but by tether relaxation motions and cross-link densities. Mechanical properties are also dominated by tether structures and properties, while they are governed by the rule of mixtures in silica-filled epoxies. Because epoxy cube nanocomposites are homogeneous and can be processed as organic epoxies, they can be further modified by silica particles or sol-gel methods to form three component hybrid systems to further improve properties. In a separate paper to be submitted shortly, we will demonstrate the concept of modifying composites at nano and macro lengths scale to improve multiple properties simultaneously and independently.⁷⁸

X-ray Diffraction (XRD). The ordering of cubes in the networks was studied using XRD. Figure 18 compares the powder patterns of the OC monomer with OC/DDM nanocomposites at various N 's. The OC monomer exhibits peaks at ~ 7.0 and 8.8° 2θ corresponding to repeat distances of approximately 1.3 and 1.0 Å, which are likely unit cell dimensions, as reported in the literature.^{79–81} A peak at 18.0° corresponding to 0.5 nm may originate from higher order diffraction of cube unit cells or from Si–O–Si linkages within the cubes. These peaks broaden on incorporating OC in epoxy resin systems. The peaks at ~ 7.0 and 8.8° are replaced by a broad single peak (peak I). The peak at 18.0° shifts slightly to lower 2θ values (peak II). The high peak intensities suggest that significant ordering exists in the networks. Small shoulders at 22 – 28° suggest that amorphous regions also exist.

As N increases, the intensity of peak I decreases somewhat, the line broadens, and most importantly shifts to higher 2θ , corresponding to shortening of the repeat distance by ~ 1 Å. This change is likely related to the change in elastic modulus that occurs simultaneously which must occur by some increase in ordering of the segment chains. As noted above this may occur

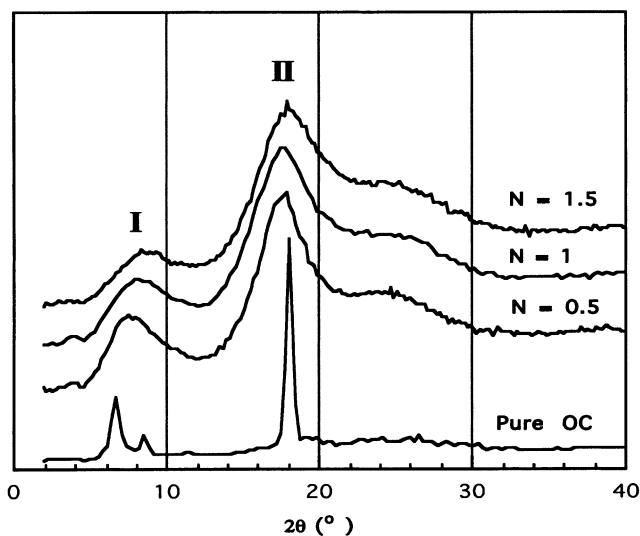


Figure 18. XRDs of OC monomer and OC/DDM nanocomposites at various N 's.

by an “unraveling” of the segment causing better alignment of chain segments. The change in periodicity with this proposed segmental reordering supports the above explanation but remains incomplete.

Note that the net silica contents at $N=0.5$, 1.0 , and 1.5 are ~ 34 , 28 , and 24 wt % respectively. OC loadings are 83.6 , 71.7 , and 62.8 wt % respectively. Because peak I is likely associated with cube-to-cube distances, its shift to higher 2θ values suggests that the cubes are more densely packed as less OC and more DDM are used. This is very surprising because these results suggest that OC cubes accommodate more DDM and at the same time they are closer to each other at high N 's. This is possible only if tether configurations change to generate more space between cubes as N increases (at least along one dimension) and more DDM terminated pendant groups form but become closer in other dimensions. These results seem to support our argument that tethers prefer linear formation at high N 's. However, more in-depth understanding of the changes in cube ordering related to changes in macroscopic properties needs further investigation, and will be conducted in the future. In comparison, the intensity and breadth of peak II barely change as N changes. Unfortunately, the origin of this peak in the cross-linked cubes is not well-understood yet, and it needs further study.

Recent work by Mather et al., Lee and Lichtenhan have demonstrated that the introduction of silsesquioxane end groups onto thermoplastic organic polymer chains has a novel effect on crystallization behavior, improves heat deflection temperatures, and in some instances viscoelastic behavior.^{83,84} These effects are reported to be at least in part, the influence of the highly massive end groups on segment motion. While it would be attractive to compare their work with the work reported here, the polymer segment sizes in the Mather, Lee, and Lichtenhan papers are far larger (e.g., minimum of 15 monomer units for Mather work) than the single segment tethers described here and are for thermoplastic materials. The materials reported here are thermosets with some of the highest cross-link densities ever reported, leading to segment motion so highly constrained that it is difficult to make a reasonable comparison.

Conclusions

The comparative study of OC/DDM and OG/DDM systems provide several conclusions for epoxy-cube nanocomposite systems and their structure–property relationships. At the same time, these conclusions can be expected to be useful as general guidelines for further development of various polymer-cube nanocomposites.

First, this study establishes standard research protocols for general cube nanocomposites studies. This study demonstrates the formation of well-defined nanocomposites from selectively designed functionalized cubic silsesquioxanes, systematic assessment of their physical properties and quantitative analysis of nanoarchitectures.

Second, cube nanocomposites are very homogeneous with no phase segregation even at nm scale. Organic and inorganic components are uniformly distributed forming one thermodynamic phase and thus the properties of the resulting nanocomposites can be expected to be isotropic. This observation suggests that nanocomposites prepared from any polyfunctional cubes must be homogeneous if the tether lengths are of the same order as the size of the silica core.

Third, this study provides the first detailed proof that nanoscale modification in thermoset nanocomposites can affect macroscale properties significantly. It further suggests that macroscopic properties are a combination of well-defined individual tether properties and thus can represent single tether behavior. Furthermore, individual cube nanocomposites exhibit nonlinear property changes vs tether manipulation, and it appears that modeling studies can be used to provide detailed information about properties and eventually to predict properties. In this work, rigid tethers provide better thermomechanical stabilities at the expense of fracture toughness vs linear ones.

Finally, blending seems to permit effective optimization of properties. On blending, new properties result that appear not to be determined by the rule of the mixtures, but rather by the specific tethers used. While blending is common practice in epoxy resin optimization, we believe that our studies provide the opportunity to clearly explain the effects of blending on macroscopic properties based on nanoscale design and processing. We believe this is an added benefit to developing nanocomposite materials with completely defined interfaces.

In an ongoing study, other parameters such as tether length, chemical structure and cross-linking chemistry will be varied and their effects on the nanocomposite properties investigated. On the basis of the conclusions above, following studies will introduce rigid aromatic segments in tethers to develop high-temperature nanocomposites and study the tether chemical structure–property relationships. Additionally, various functional groups including imides are being explored to provide a set of nanocomposites for comparative study. In work to be published separately, all these concepts will be demonstrated.

Acknowledgment. We thank the FAA, AOARD, AFOSR, and Matsushita Electric for generous support of this work. We would especially like to thank Dr. I. Lee for the theoretical modeling studies.²⁸

References and Notes

- (1) Sanchez, C.; Soler-Illa, G. J. de A. A.; Lalot, T.; Maayer, C. R.; Cabuil, V. *Chem. Mater.* **2001**, *13*, 3061.

- (2) Sanchez, C.; Lebeau, B. *MRS Bull.* **2000**, *26*, 377.
- (3) Rajeshwar, K.; de Tacconi, N. R.; Chenthamarakshan, C. R. *Chem. Mater.* **2001**, *13*, 2765.
- (4) Pyun, J.; Matyjaszewski, K. *Chem. Mater.* **2001**, *13*, 3436.
- (5) Gomez-Romero, P. *Adv. Mater.* **2001**, *13*, 163.
- (6) Seraji, S.; Wu, Y.; Forbess, M.; Limmer, S. J.; Chou, T.; Cao, G. *Adv. Mater.* **2000**, *12*, 1695.
- (7) Matejka, L.; Dukh, O. *Macromol. Symp.* **2001**, *171*, 181.
- (8) Scott, B. J.; Wirnsberger, G.; Stucky, G. D. *Chem. Mater.* **2001**, *13*, 3140.
- (9) Alexandre, M.; Dubois, P. *Mater. Sci. Eng.* **2000**, *28*, 1.
- (10) PeBaron, P. C.; Wang, Z.; Pinnavaia, T. J. *Appl. Clay Sci.* **1999**, *15*, 11.
- (11) Kojima, Y.; Usuki, A.; Kawasumi, M. *J. Mater. Res.* **1993**, *8*, 1185.
- (12) Kojima, Y.; Usuki, A.; Kawasumi, M.; Okada, A.; Kurauchi, T.; Kamigaito, O. *Mater. Life* **1993**, *5*, 13.
- (13) Burnside, S. D.; Giannelis, E. P. *Chem. Mater.* **1995**, *7*, 1597.
- (14) Vaia, R. A.; Price, G.; Ruth, P. N.; Nguyen, H. T.; Lichtenhan, J. *Appl. Clay Sci.* **1999**, *15*, 67.
- (15) Lan, T.; Kaviratna, P. D.; Pinnavaia, T. J. *Chem. Mater.* **1994**, *6*, 573.
- (16) Yano, K.; Usuki, A.; Okada, A. *J. Polym. Sci., Part A: Polym. Chem.* **1997**, *35*, 2289.
- (17) Tsai, M.; Whang, W.-T. *Polymer* **2001**, *42*, 4197.
- (18) Lan, J. K.; Wang, Y. L.; Wu, Y. L.; Liou, H. C.; Wang, J. K.; Chiu, S. Y.; Cheng, Y. L.; Feng, M. S. *Thin Solid Films* **2000**, *377–378*, 776.
- (19) Harkness, B. R.; Takeuchi, K.; Tachikawa, M. *Macromolecules* **1998**, *31*, 4798.
- (20) Rottman, C.; Grader, G.; DeHazan, Y.; Melchior, S. Avnir, D. *J. Am. Chem. Soc.* **1999**, *121*, 8533.
- (21) Wirnsberger, G.; Scoott, B. J.; Chmelka, B. F.; Stucky, G. D. *Adv. Mater.* **2000**, *12*, 1450.
- (22) Dantas De Moraes, T.; Chaput, F.; Boilot, J.-P.; Lahlil, K.; Darracq, B.; Levy, Y. *Adv. Mater.* **1999**, *11*, 107.
- (23) Schaudel, B.; Guermur, C.; Sanchez, C.; Nakatani, K.; Delaire, J. *J. Mater. Chem.* **1997**, *7*, 61.
- (24) Ribot, F.; Eychenne-Baron, C.; Sanchez, C. *Phosphorus Sulfur Silicon Relat. Elem.* **1999**, *150–151*, 41.
- (25) Mayer, C. R.; Fournier, I.; Thouvenot, R. *Chem.—Eur. J.* **2000**, *6*, 105.
- (26) Mayer, C. R.; Herson, P.; Thouvenot, R. *Inorg. Chem.* **1999**, *38*, 6152.
- (27) Morosin, B. *Acta Crystallogr. B* **1997**, *33*, 303.
- (28) Laine, R. M.; Choi, J.; Lee, I. *Adv. Mater.* **2001**, *13*, 800.
- (29) Choi, J.; Harcup, J.; Yee, A. F.; Zhu, Q.; Laine, R. M. *J. Am. Chem. Soc.* **2001**, *123*, 11420.
- (30) Tamaki, R.; Tanaka, Y.; Asuncion, M. Z.; Choi, J.; Laine, R. M. *J. Am. Chem. Soc.* **2001**, *123*, 12416.
- (31) Zhang, C.; Babonneau, F.; Bonhomme, C.; Laine, R. M.; Soles, C. L.; Hristov, H. A.; Yee, A. F. *J. Am. Chem. Soc.* **1998**, *120*, 8380.
- (32) Zhang, C.; Laine, R. M. *J. Am. Chem. Soc.* **2000**, *122*, 6979.
- (33) Sellinger, A.; Laine, R. M. *Macromolecules* **1996**, *29*, 2327.
- (34) Zhang, C.; Laine, R. M. *J. Organomet. Chem.* **1996**, *521*, 199.
- (35) Sellinger, A.; Laine, R. M. *Chem. Mater.* **1996**, *9*, 1592.
- (36) Laine, R. M.; Zhang, C.; Sellinger, A.; Viculis, L. *Appl. Organomet. Chem.* **1998**, *12*, 715.
- (37) Large-Toumi, B.; Salvia, M.; Vincent, M. In *Fiber, matrix, and interface properties*; ASTM STP 1290; Spragg, C. J., Dzal, L. T., Eds.; ASTM: Philadelphia, PA, 1996; p 182.
- (38) Li, T.; Zhang, K.; Zeng, H. *Compos. Sci. Technol.* **2000**, *60*, 465.
- (39) Apfel, M. A.; Finkelmann, H.; Janni, G. M.; Laub, R. J.; Lüthmann, B.-H.; Price, A.; Roberts, W. L.; Shaw, T. J.; Smith, C. A. *Anal. Chem.* **1985**, *57*, 651.
- (40) Tanaka, Y. In *Epoxy resins, chemistry and technology*; May, C. A., Ed.; Marcel Dekker: New York, 1988; p 9.
- (41) Goodman, S. H. In *Handbook of thermoset plastics*; Goodman, S. H., Ed.; Noyes Publ.: Westwood, NJ, 1998; p 193.
- (42) Smith, G.; May, C. A. In *Epoxy resins*; Gould, R. F., Ed.; American Chemical Society: Washington, DC, 1970; p 140.
- (43) Cardwell, B. J.; Yee, A. F. *J. Mater. Sci.* **1998**, *33*, 5473.
- (44) Vanlandingham, M. R.; Eduljee, R. F.; Gillespie, L. W., Jr. *J. Appl. Polym. Sci.* **1999**, *71*, 699.
- (45) Costa, R. O. R.; Tamaki, R.; Vasconcelos, W. L.; Laine, R. M.; *Macromol.* **2001**, *34*, 5398–5407.
- (46) Marcolli, C.; Calzaferri, G. *Appl. Organomet. Chem.* **1999**, *13*, 213.
- (47) Wallace, W. E.; Guttman, C. M.; Antonucci, J. M. *Polymer* **2000**, *41*, 2219.
- (48) Chen, Y.; Iroh, J. O. *Chem. Mater.* **1999**, *11*, 1222.

- (49) Silverstein, R. M.; Webster, F. X. *Spectrometric identification of organic compounds*; John Wiley & Sons: New York, 1996; p 71.
- (50) Deng, B.; Hu, Y.; Chen, L.; Chiu, W.; Wu, T. *J. Appl. Polym. Sci.* **1999**, *74*, 229.
- (51) Hwang, S. H.; Jung, J. C. *J. Appl. Polym. Sci.* **2001**, *81*, 279.
- (52) Matsumoto, T. *Macromolecules* **1999**, *32*, 4933.
- (53) Wang, L.; Wong, C. P. *J. Polym. Sci., Part A* **1999**, *37*, 2991.
- (54) Wang, L.; Li, H.; Wong, C. P. *J. Polym. Sci., Part A* **2000**, *38*, 3771.
- (55) Choi, J.; Laine, R. M. Unpublished work.
- (56) Dyakonov, T.; Mann, P. J.; Chen, Y.; Stevensen, W. T. K. *Polym. Degrad. Stab.* **1996**, *54*, 67.
- (57) Engelberg, P. I.; Tesoro, G. C. *Polym. Eng. Sci.* **1990**, *30*, 303.
- (58) Martin, D. C.; Thomas, E. L. *Polymer* **1995**, *36*, 1759.
- (59) Choi, J.; Yee, A. F.; Laine, R. M. Organic/inorganic hybrid epoxy composites from aminophenylsilsesquioxanes. Manuscript submitted.
- (60) Kim, S. L.; Skibo, M. D.; Manson, J. A.; Hertzberg, R. W.; Janiszewski, J. *Polym. Eng. Sci.* **1978**, *18*, 1093.
- (61) Bellenger, V.; Dhaoui, W.; Ensam, J. V. *Polym. Eng. Sci.* **1990**, *30*, 321.
- (62) Palmese, G. R.; McCullough, R. L. *J. Appl. Polym. Sci.* **1992**, *46*, 1863.
- (63) Vanlandingham, M. R.; Eduljee, R. F.; Gillespie, J. W., Jr. *J. Appl. Polym. Sci.* **1999**, *71*, 699.
- (64) Skourlis, T. P.; McCullough, R. L. *J. Appl. Polym. Sci.* **1996**, *62*, 481.
- (65) Shih, W. C.; Ma, C. C. M.; Yang, J. C.; Chen, H. D. *J. Appl. Polym. Sci.* **1999**, *73*, 2739.
- (66) Matejka, L. Dukh, O.; Kolarik, J. *Polymer* **2000**, *41*, 1449.
- (67) Ochi, M.; Takahashi, R. *J. Polym. Sci., Part B: Polym. Phys.* **2001**, *39*, 1071.
- (68) Hsiue, G. H.; Liu, Y. L.; Liao, H. H. *J. Polym. Sci., Part A: Polym. Chem.* **2001**, *39*, 986.
- (69) Hsiue, G. H.; Wang, W. J.; Chang, F. C. *J. Appl. Polym. Sci.* **1999**, *73*, 1231.
- (70) Okazaki, M.; Murota, M.; Kawaguchi, Y.; Tsubokawa, N. *J. Appl. Polym. Sci.* **2001**, *80*, 573.
- (71) Kang, S.; Hong, S.; Choe, C.; Park, M.; Rim, S.; Kim, J. *Polymer* **2001**, *42*, 879.
- (72) Nakamura, Y.; Yamaguchi, M.; Okubo, M.; Matsumoto, T. *J. Appl. Polym. Sci.* **1992**, *44*, 151.
- (73) Nakamura, Y.; Yamaguchi, M. *Polymer* **1992**, *33*, 3415.
- (74) Koh, S.-W.; Kim, J. K.; Mai, Y. W. *Polymer* **1993**, *34*, 3446.
- (75) Wong, C. P.; Bollampally, R. S. *J. Appl. Polym. Sci.* **1999**, *74*, 3396.
- (76) Kaelble, D. H. In *Epoxy resins, chemistry and technology*; May, C. A., Ed.; Marcel Dekker: New York, 1988; p 603.
- (77) Wang, J. *Microelectron. Reliab.* **2002**, *42*, 293.
- (78) Choi, J.; Yee, A. F.; Laine, R. M. Toughening of cubic silsesquioxane epoxy nanocomposites using core shell rubber; a three component hybrid system. Manuscript submitted.
- (79) Romo-Uribe, A.; Mather, P. T.; Haddad, T. S.; Lichtenhan, J. D. *J. Polym. Sci., Part B: Polym. Phys.* **1998**, *36*, 1857.
- (80) Prado, L. A. S. De A.; Radovanovic, E.; Pastore, H. O.; Yoshida, I. V. P.; Torriani, I. L. *J. Polym. Sci., Part B: Polym. Phys.* **2000**, *38*, 1580.
- (81) Larsson, K. *Ark. Kem.* **1960**, *16*, 203.
- (82) Choi, J.; Tamaki, R.; Laine, R. M. *Chem. Mater.* **2003**, *15*, 793.
- (83) Kim, B.-S.; Mather, P. T. *Macromolecules* **2002**, *35*, 8378.
- (84) Lee, A.; Lichtenhan, J. D. *Macromolecules* **1998**, *31*, 4970.

MA030172R